Plant Communications
Research Article

CellPress
Partner Journal

A *Phelipanche ramosa* KAI2 protein perceives strigolactones and isothiocyanates enzymatically

Alexandre de Saint Germain[1], Anse Jacobs[2,3,4,5], Guillaume Brun[6,7], Jean-Bernard Pouvreau[6], Lukas Braem[2,3,4,5], David Cornu[8], Guillaume Clavé[9], Emmanuelle Baudu[1], Vincent Steinmetz[9], Vincent Servajean[9], Susann Wicke[7], Kris Gevaert[4,5], Philippe Simier[6], Sofie Goormachtig[2,3], Philippe Delavault[6] and François-Didier Boyer[9,*]

[1]Institut Jean-Pierre Bourgin, INRAE, AgroParisTech, Université Paris-Saclay, 78000 Versailles, France

[2]Department of Plant Biotechnology and Bioinformatics, Ghent University, 9052 Gent, Belgium

[3]Center for Plant Systems Biology, VIB, 9052 Gent, Belgium

[4]Department of Biomolecular Medicine, Ghent University, 9000 Ghent, Belgium

[5]Center for Medical Biotechnology, VIB, 9000 Ghent, Belgium

[6]Laboratoire de Biologie et Pathologie Végétales (LBPV), Equipe d'Accueil 1157, Université de Nantes, 44000 Nantes, France

[7]Institute for Biology, Humboldt-Universität zu Berlin, 10115 Berlin, Germany

[8]Université Paris-Saclay, CEA, CNRS, Institute for Integrative Biology of the Cell (I2BC), 91198, Gif-sur-Yvette, France

[9]Université Paris-Saclay, CNRS, Institut de Chimie des Substances Naturelles, UPR 2301, 91198, Gif-sur-Yvette, France

***Correspondence: François-Didier Boyer (francois-didier.boyer@cnrs.fr)**

https://doi.org/10.1016/j.xplc.2021.100166

ABSTRACT

***Phelipanche ramosa* is an obligate root-parasitic weed that threatens major crops in central Europe. In order to germinate, it must perceive various structurally divergent host-exuded signals, including isothiocyanates (ITCs) and strigolactones (SLs). However, the receptors involved are still uncharacterized. Here, we identify five putative SL receptors in *P. ramosa* and show that PrKAI2d3 is involved in the stimulation of seed germination. We demonstrate the high plasticity of PrKAI2d3, which allows it to interact with different chemicals, including ITCs. The SL perception mechanism of PrKAI2d3 is similar to that of endogenous SLs in non-parasitic plants. We provide evidence that PrKAI2d3 enzymatic activity confers hypersensitivity to SLs. Additionally, we demonstrate that methylbutenolide-OH binds PrKAI2d3 and stimulates *P. ramosa* germination with bioactivity comparable to that of ITCs. This study demonstrates that *P. ramosa* has extended its signal perception system during evolution, a fact that should be considered for the development of specific and efficient biocontrol methods.**

Keywords: α/β-hydrolase, receptor, seed germination stimulant, strigolactones, isothiocyanates, *Phelipanche ramosa*

de Saint Germain A., Jacobs A., Brun G., Pouvreau J.-B., Braem L., Cornu D., Clavé G., Baudu E., Steinmetz V., Servajean V., Wicke S., Gevaert K., Simier P., Goormachtig S., Delavault P., and Boyer F.-D. (2021). A *Phelipanche ramosa* KAI2 protein perceives strigolactones and isothiocyanates enzymatically. Plant Comm. **2**, 100166.

INTRODUCTION

Witchweeds (*Striga* spp.) and broomrapes (*Orobanche* and *Phelipanche* spp.) are obligate root-parasitic plants of the Orobanchaceae family that together comprise the most threatening weeds for major domesticated crops worldwide (Parker, 2012). At maturity, a single plant releases up to 100 000 microscopic seeds, resulting in severe soil pollution (Delavault et al., 2017). Seed germination of these obligate parasites requires the strict recognition of host-exuded germination stimulants. Broomrapes and witchweeds are all highly sensitive to strigolactones (SLs) secreted by plants into the rhizosphere at picomolar doses (Brun et al., 2017). The structural core of SLs is a tricyclic lactone, referred to as the ABC part in canonical SLs or as a structural variant in non-canonical SLs. It is invariably connected to an α,β-unsaturated furanone moiety (the D ring) by an enol ether bridge (Supplemental Figure 1A) (Brun et al., 2017). Some

Published by the Plant Communications Shanghai Editorial Office in association with Cell Press, an imprint of Elsevier Inc., on behalf of CSPB and CEMPS, CAS.

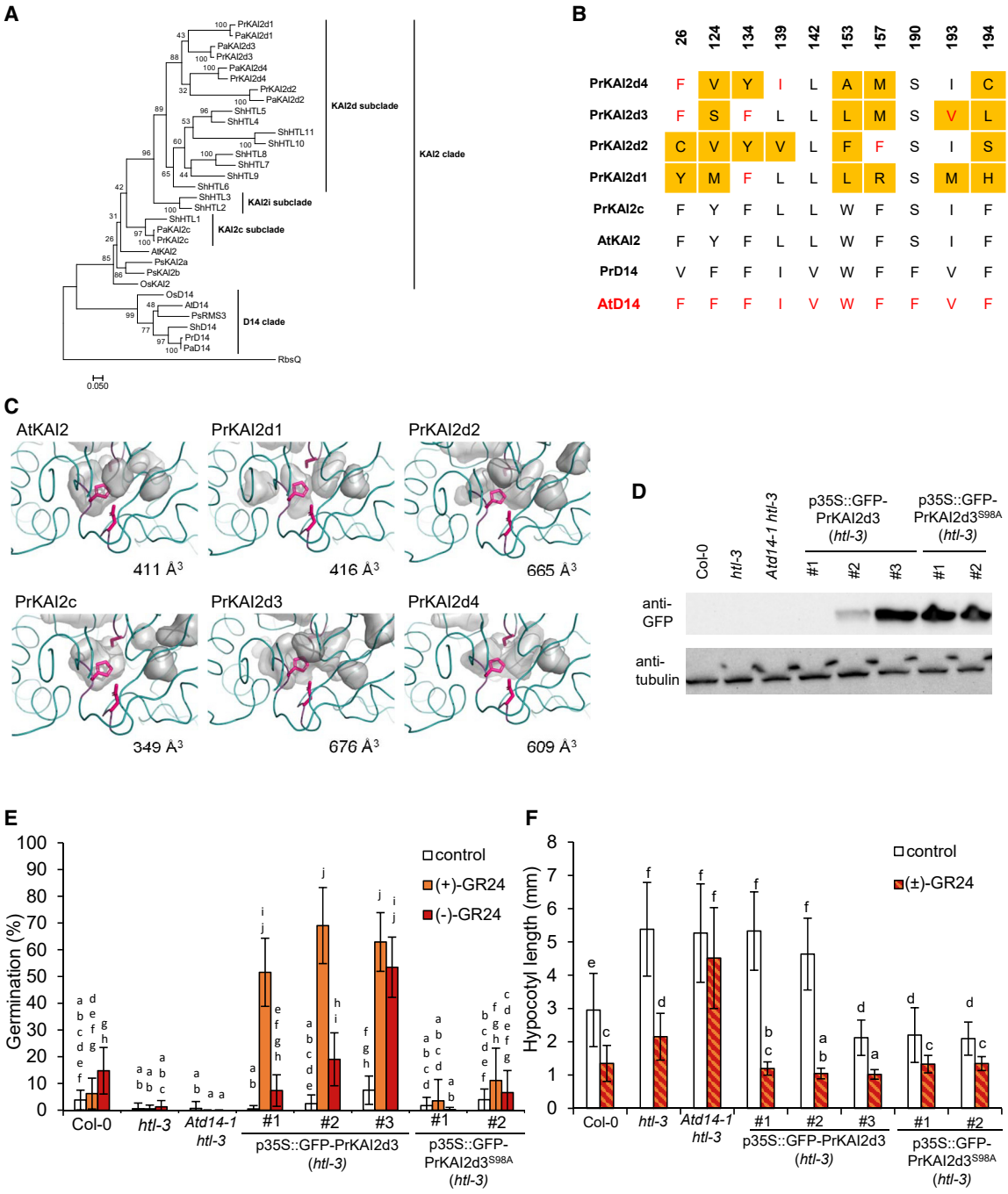

Figure 1. Identification of PrKAI2 putative SL receptors in *P. ramosa*.

(A) Phylogenetic analysis of KAI2 and D14 amino acid sequences. The phylogenetic tree was constructed with the ML method and 1000 bootstrap replicates using RAxML. The scale bar represents 0.05 substitutions per site. Clades were designated as described previously (Conn et al., 2015).

(B) Amino acid sequence alignment of the active PrKAI2 protein sites. Amino acids that differ from AtKAI2 and those similar to AtD14 are in orange and red, respectively; AtHTL and PrKAI2d3 are in blue and yellow, respectively. A fully expanded alignment can be found in Supplemental Figure 3.

(C) Visual representation of the ligand pockets of the *P. ramosa* KAI2 proteins. The KAI2 protein sequences were modeled using chain A of the karrikin-bound *Arabidopsis* KAI2 structure as a template (PDB: 4JYP). The protein structures were generated with PyMOL, and the cavities within the homology models are shown as a semitransparent surface. Catalytic residues (Ser, His, Asp) are shown in stick representation.

(D–F) Cross-species complementation assays of the *htl-3* mutant with *P. ramosa* KAI2d3 and the catalytic site mutant S98A. **(D)** PrKAI2d3 protein levels of 4-day-old seedlings transformed with *p35S::GFP-PrKAI2d3* or *p35S::GFP-PrKAI2d3^{S98A}* detected with anti-GFP (top) and anti-tubulin (bottom) antibodies as a loading control. The experiment was repeated twice with comparable results, and one representative replicate is shown. **(E)** Seed germination

(legend continued on next page)

germination stimulants are exclusive to specific host-parasite interactions, as illustrated by the unique ability of *Phelipanche ramosa* to germinate upon sensing isothiocyanates (ITCs). These glucosinolate breakdown products are exuded by rapeseed (*Brassica napus*) (Auger et al., 2012; Delavault et al., 2017), to which *P. ramosa* has adapted in a decade (Parker, 2012; Delavault et al., 2017). Broomrapes are increasingly problematic in both intensity and acreage in Europe, North Africa, and Asia, and they are expected to dramatically expand to new territories in the near future (Grenz and Sauerborn, 2007). To date, several physical, cultural, chemical, and biological approaches have been explored to control root-parasitic weeds, but no method has been found completely satisfactory (Fernandez-Aparicio et al., 2016).

In addition to their involvement in germination, SLs strongly stimulate arbuscular mycorrhizal fungi (Glomeromycotina) by promoting mitochondrial metabolism and hyphal branching (Besserer et al., 2008), thereby mediating the establishment of the oldest mutualistic interaction of land plants (Brundrett and Tedersoo, 2018). In addition to their role in rhizosphere signaling, SLs also act as hormones *in planta* and have pervasive roles throughout plant development (Lopez-Obando et al., 2015). As such, they are perceived by the α/β-hydrolase DWARF14 (D14) in vascular plants (Hamiaux et al., 2012; Waters et al., 2017). Biochemical analyses with recombinant D14 proteins by means of the synthetic SL analog GR24 revealed that SL signal transduction requires GR24 cleavage (Nakamura et al., 2013; Waters et al., 2017). One of the cleavage products, the D ring, may remain covalently attached to the receptor (de Saint Germain et al., 2016; Yao et al., 2016), thereby probably allowing the recruitment of partners for downstream processes (Shabek et al., 2018). The requirement of SL cleavage for signal transduction is still under debate (Shabek et al., 2018; Seto et al., 2019).

In *Arabidopsis thaliana*, D14 belongs to a small protein family, including KARRIKIN INSENSITIVE2/HYPOSENSITIVE TO LIGHT (AtKAI2/AtHTL), that shares the α/β-hydrolase catalytic triad. However, AtKAI2 regulates AtD14-independent processes such as seed germination and preferentially perceives (−)-GR24, which mimics non-natural SLs, karrikins (Sun et al., 2016), and supposedly an unknown endogenous ligand (Conn and Nelson, 2016; Swarbreck et al., 2019; Villaécija-Aguilar et al., 2019). Interestingly, the *KAI2* gene family has expanded during the genome evolution of obligate parasitic plants (Conn et al., 2015). For example, *Phelipanche aegyptiaca* and *Striga hermonthica* possess five and eleven *KAI2*/*HTL* genes, respectively. Two *KAI2* paralogs play a role in the SL response of *P. aegyptiaca* (Conn et al., 2015), and six *S. hermonthica* KAI2/HTL proteins are hypersensitive to SLs (Conn et al., 2015; Toh et al., 2015), with ShHTL7 exhibiting the same perception mechanism as D14 (Yao et al., 2017). The remarkable expansion of the *KAI2* gene family in Orobanchaceae, along with the capacity of *P. ramosa* to perceive ITCs, led us to speculate that KAI2 proteins may also perceive other germination stimulants. Here, we characterize PrKAI2d3 as a *P. ramosa* SL receptor. We demonstrate that it is able to perceive natural SLs by an enzymatically dependent mechanism that contributes to its SL hypersensitivity. We also show that PrKAI2d3 perceives ITCs as well as a wide range of SL analogs that were not found to be bioactive for SL hormonal functions. Together, these results suggest that PrKAI2 proteins evolved as hypersensitive and plastic receptors, enabling the parasitic plant to detect various host exudate metabolites and contributing to its dramatic success.

RESULTS

Identification and gene expression profiles of PrKAI2 homologs

Iterative nucleotide and amino acid BLAST analyses were performed on the recently published transcriptome of the *P. ramosa* rapeseed strain (Goyet et al., 2017) using known *KAI2* and *D14* sequences from non-parasitic and parasitic plants as queries (Conn et al., 2015; Toh et al., 2015). Each newly identified sequence was used as a query for new BLAST searches in order to find all complete sequences, and duplicates were eliminated before alignment. One *PrD14* and five *PrKAI2* putative orthologs were identified, amplified, and re-sequenced from cDNA isolated from germinated seeds of the same *P. ramosa* strain. Maximum-likelihood (ML) phylogenetic analysis indicated that the predicted PrD14 and PrKAI2 proteins (Figure 1A) and genes (Supplemental Figure 2) belonged to clearly distinct D14 and KAI2 clades. They possessed a conserved catalytic triad and an overall conserved environment of known active-site amino acid residues (Supplemental Figure 3). Despite the poor separation of the non-parasitic and parasitic KAI2 groups, the phylogenetic analysis strongly suggested that none of the retrieved PrKAI2 proteins belonged to the intermediate KAI2i subclade (Figure 1A), as previously described for other members of the *Orobanche* and *Phelipanche* genera (Conn et al., 2015). The newly identified PrKAI2 and PrD14 proteins consistently clustered together with *P. aegyptiaca* sequences. Together with the low levels of genomic divergence reported in *Phelipanche* (Wicke et al., 2016; Yang et al., 2016), these findings hint at the detection of *P. aegyptiaca* protein orthologs. Hence, the *P. ramosa* sequences were renamed according to the current nomenclature (Conn et al., 2015), with one PrKAI2 protein belonging to the conserved KAI2 (PrKAI2c) clade and four PrKAI2 proteins assigned to the divergent KAI2 clade (PrKAI2d1–d4).

PrKAI2d3 is a putative SL receptor

By comparing amino acid residues in the PrKAI2 ligand-binding pocket to those from AtD14 and AtKAI2, we found that PrKAI2d3 exhibited the highest similarity to AtD14 (Figure 1B). Predictive models generated with the SWISS-MODEL

after 5 days of growth at 25°C in the dark with DMSO (control), 10 μM (+)-GR24, or 10 μM (−)-GR24 treatment. Transgenes were expressed in the null *htl-3* mutant background (Col-0 accession) under the control of the 35S promoter. One representative experiment of 18 wells per condition with an average of 19 seeds/well is shown. **(F)** Hypocotyl lengths of 4-day-old seedlings grown under continuous red light at 21°C ($n = 25$) with 10 μM (±)-GR24 treatments. Graphs show the means ± SE of three biological replicates. Statistical groups indicated by letters were determined by the Kruskal–Wallis test with Dunn's post-hoc test, $p < 0.001$ **(E)** and $p < 0.05$ **(F)**.

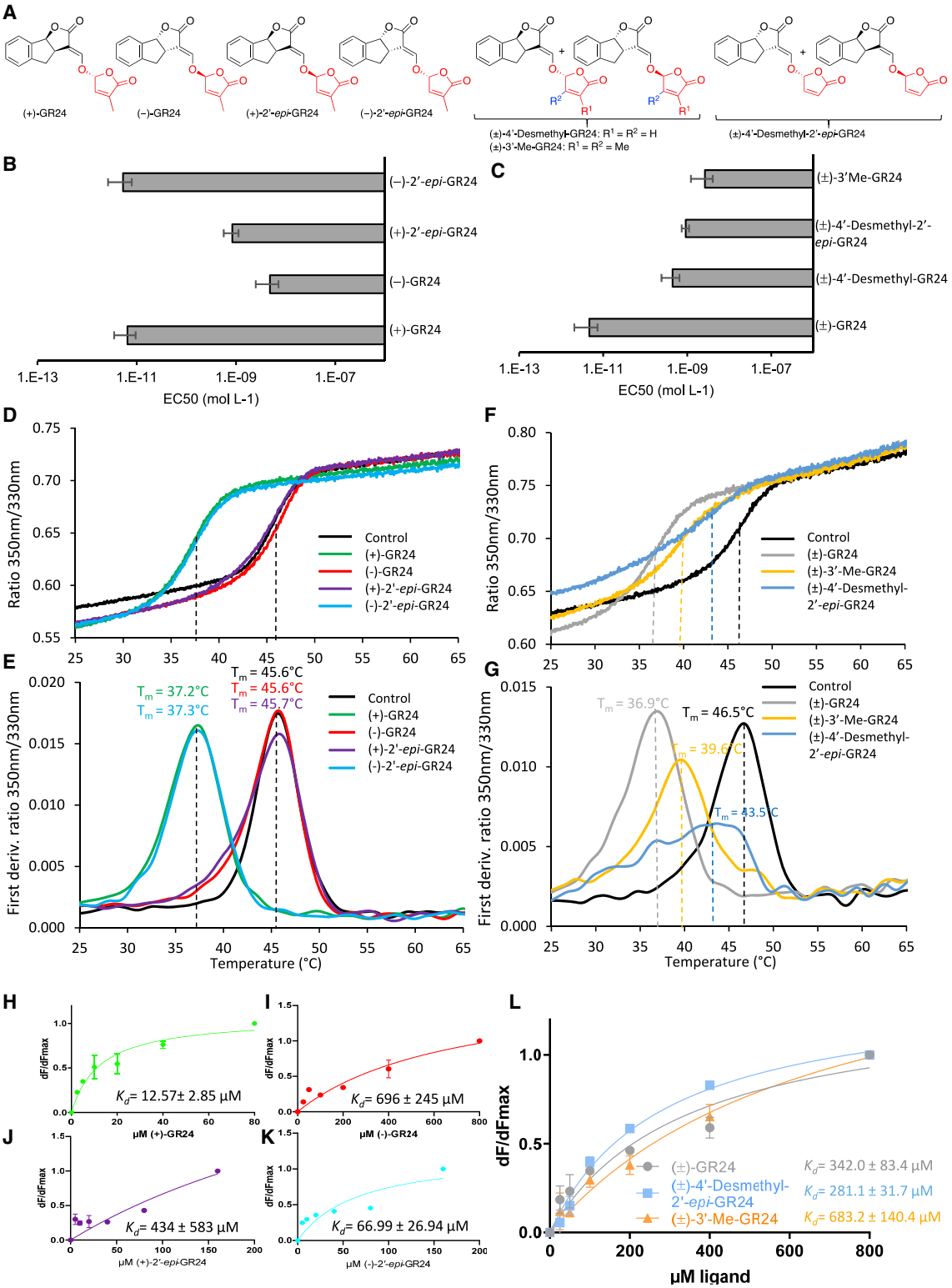

Figure 2. PrKAI2d3 shows stereoselectivity toward GR24 analogs mimicking the SL natural stereoconfigurations and perceives SL analogs without a methyl group on the D ring.

(A) Structures of GR24 analogs.

(B and C) Germination stimulation activity on *P. ramosa* seeds (EC_{50}) of four stereoisomers and of GR24 analogs harboring variations on the D ring (± SE).

(legend continued on next page)

webserver revealed that the binding pocket of PrKAI2c is smaller than that of AtKAI2 (Figure 1C) and that the PrKAI2d protein binding pockets are wider than those of members of the conserved KAI2 clade, probably because of the absence of large hydrophobic residues (Figure 1C). Among all the divergent proteins, PrKAI2d3 had the largest predicted binding pocket (Figure 1C, Supplemental Figure 4). The levels of all four *PrKAI2d* transcripts in *P. ramosa* seeds changed significantly after 6 h of treatment with exogenous (±)-GR24 and 2-PEITC (phenethyl isothiocyanate) (Supplemental Figure 5). By contrast, the transcript levels of PrKAI2c, which is putatively orthologous to AtKAI2, remained unchanged. Based on these data, all the PrKAI2ds may be involved in SL perception and should be considered further for complete biochemical and physiological characterization. In our attempt to characterize all PrKAI2d recombinant proteins, we managed to produce only recombinant PrKAI2d3; the other proteins remained non-soluble under our experimental conditions. As a result, we will focus here on the characterization of PrKAI2d3 at the biochemical and physiological levels.

Because no mutants or simple and rapid transformation methods are available for holoparasitic Orobanchaceae, it is difficult (Fernández-Aparicio et al., 2011) to validate the biological function of PrKAI2d3 directly in *P. ramosa*. Instead, we assayed the complementation of the *Arabidopsis htl-3* mutant phenotype with PrKAI2d3, a previously successful approach (Conn et al., 2015; Toh et al., 2015). To assess the role of the catalytic triad in the perception process, *htl-3* was also transformed with a mutated gene that encoded PrKAI2d3^{S98A}. We recorded germination and hypocotyl length phenotypes in three p35S::GFP-PrKAI2d3 lines that displayed various protein levels and two p35S::GFP-PrKAI2d3^{S98A} lines that showed high protein expression (Figure 1D).

In a thermo-inhibition assay (Toh et al., 2012), almost no germination was detected in all lines under control treatments. Germination of *Arabidopsis* (accession Columbia-0 [Col-0]) seeds was significantly stimulated by 10 μM (−)-GR24 but not by (+)-GR24, whereas none of the enantiomers had an effect on the germination of the *htl-3* or *Atd14-1/htl-3* mutants (Figure 1E). Germination of all three p35S::GFP-PrKAI2d3 lines was strongly induced by (+)-GR24. Exogenous (−)-GR24 also significantly stimulated germination of these three lines (Figure 1E), and the response amplitude was positively correlated with protein abundance (Figure 1D). Analysis of a fourth p35S::GFP-PrKAI2d3 line showed that even low PrKAI2d3 protein expression increased *Arabidopsis* sensitivity toward (−)-GR24 100-fold, enabling it to perceive picomolar doses of (+)-GR24 and, hence, to have *P. ramosa* levels of sensitivity (Figure 2A and 2B, Supplemental Figure 6, Supplemental Table 1). Neither of the two p35S::GFP-PrKAI2d3^{S98A} lines were sensitive to (+)- or (−)-GR24.

Under red light conditions, the hypocotyls of *htl-3* and *Atd14-1/htl-3* mutants are more elongated than those of Col-0 (Waters et al., 2012) (Figure 1F). Application of (±)-GR24 significantly shortened the hypocotyls of Col-0 and the *htl-3* genotypes, but had no effect on those of the *Atd14-1/htl-3* plants. This observation corroborates a previous report that *Arabidopsis* seedling photomorphogenesis is redundantly controlled by D14 and KAI2/HTL (Waters et al., 2012). Interestingly, only hypocotyls of the p35S::GFP-PrKAI2d3 and p35S::GFP-PrKAI2d3^{S98A} lines with the highest protein levels were shorter than those of the *htl-3* and *Atd14-1/htl-3* mutants under control conditions. However, the hypocotyls were significantly shorter in all transformed lines after treatment with 1 μM (±)-GR24 (Figure 1F). In summary, these data indicate that PrKAI2d3 protein expression rescues the *htl-3* mutant phenotypes and that the catalytic Ser98 is essential for germination but not for seedling photomorphogenesis.

A structure-activity relationship study reveals that *P. ramosa* responds efficiently to SL analogs and mimics with various structures

Because *P. ramosa* perceives many germination stimulants with highly divergent structures, various receptors may underlie this plasticity (Boyer et al., 2012, 2014). To link SL structural features with *P. ramosa* seed germination activity, we performed a structure-activity relationship (SAR) study using a rapid bioassay (Pouvreau et al., 2013).

First, we determined the sensitivity of *P. ramosa* toward several GR24 analogs with varying stereogenic centers (Figure 2A). The lowest EC_{50} (half maximal effective concentration) values were obtained with (+)-GR24 (6.5 pM) and (−)-2′-*epi*-GR24 (5.3 pM), whose stereochemistry corresponds to that of natural canonical SLs of the strigol-type and orobanchol-type series, respectively (Supplemental Figure 1A). By contrast, *P. ramosa* was approximately 100-fold less sensitive to (−)-GR24 and (+)-2′-*epi*-GR24, whose stereochemistry is not encountered in natural SLs (Figure 2B, Supplemental Figure 1A).

Second, we investigated whether substitutions on the D ring altered the responses of *P. ramosa* (Boyer et al., 2012). Surprisingly, both GR24 analogs without a methyl group on the D ring, (±)-4′-desmethyl-2′-*epi*-GR24 and (±)-4′-desmethyl-GR24, significantly stimulated *P. ramosa* seed germination (EC_{50} = 0.92 and 0.45 nM), although their EC_{50} values were 100-fold lower than those of (±)-GR24 (Figure 2C). Notably, none of these substituted GR24 analogs inhibited shoot branching, even at 1 μM, above which SL analogs begin to be toxic and are no longer considered bioactive (Boyer et al., 2012). By contrast, *P. ramosa* was less sensitive to (±)-3′-methyl-GR24 (EC_{50} = 2.6 nM), which harbors two methyl groups on the D ring (Figure 2C, Supplemental Figure 7, Supplemental Table 2) and is highly bioactive in repressing pea

(D–G) Thermostability of PrKAI2d3 at 10 μM in the absence of ligands (black line) or in the presence of various ligands at 100 μM analyzed by nanoDSF. **(D)** and **(F)** The changes in fluorescence (F_{350nm}/F_{330nm} ratio) with temperature, and **(E)** and **(G)** the first derivatives of the F_{350nm}/F_{330nm} curve against the temperature gradient from which the apparent melting temperature (T_m) was determined for each sample. The experiment was performed twice.
(H–L) SL analogs binding PrKAI2d3 based on intrinsic tryptophan fluorescence. Plots of fluorescence intensity versus (+)-GR24 **(H)**, (−)-GR24 **(I)**, (+)-2′*epi*-GR24 **(J)**, (−)-2′*epi*-GR24 **(K)**, and (±)-GR24, (±)-4′-desmethyl-2′-*epi*-GR24, and (±)-3′-Me-GR24 **(L)**. The change in intrinsic fluorescence was monitored (Supplemental Figure 10) and used to determine the apparent K_D values. The plots represent the mean of two replicates, and the experiments were repeated at least three times. The analysis was performed in GraphPad Prism 7.05 software.

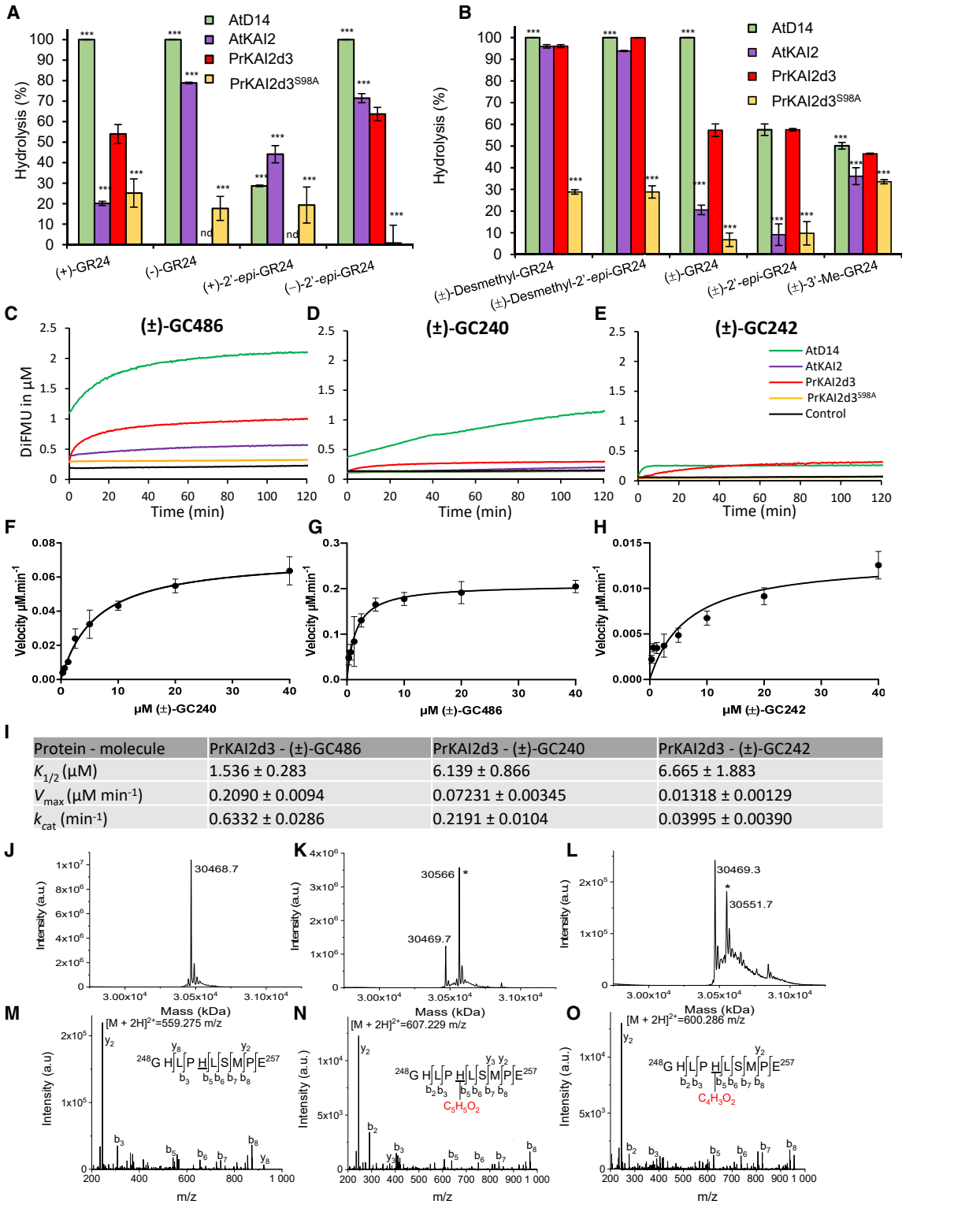

Protein - molecule	PrKAI2d3 - (±)-GC486	PrKAI2d3 - (±)-GC240	PrKAI2d3 - (±)-GC242
$K_{1/2}$ (µM)	1.536 ± 0.283	6.139 ± 0.866	6.665 ± 1.883
V_{max} (µM min^{-1})	0.2090 ± 0.0094	0.07231 ± 0.00345	0.01318 ± 0.00129
k_{cat} (min^{-1})	0.6332 ± 0.0286	0.2191 ± 0.0104	0.03995 ± 0.00390

Figure 3. The PrKAI2d3 enzymatic activity improves the SL biological activity.

(A and B) Hydrolysis activity of GR24 isomers and analogs by various proteins. (+)-GR24, (−)-GR24, (+)-2′*epi*-GR24, and (−)-2′*epi*-GR24 **(A)** and (±)-GR24, (±)-4′-desmethyl-GR24, (±)-4′-desmethyl-2′-*epi*-GR24, and (±)-3′-Me-GR24 **(B)** at 10 µM were incubated with PrKAI2d3, PrKAI2d3^{S98A}, AtD14, and AtKAI2 at 5 µM for 150 min at 25°C. UPLC-UV (260 nm) analysis was used to detect the remaining amounts of GR24 isomers and analogs. Bars represent the mean value of the hydrolysis rate calculated from the remaining GR24 isomers and analogs, taking into account the hydrolysis in the buffer alone (without protein sample) and quantified using (±)-1-indanol as an internal standard. Error bars represent the SD of three replicates (means ± SD,

(legend continued on next page)

(*Pisum sativum*) shoot branching via RMS3/PsD14 (Boyer et al., 2012; de Saint Germain et al., 2016).

Finally, we analyzed the effect of ABC-ring fragment substitution on *P. ramosa* germination using profluorescent probes in which the ABC ring was replaced by a coumarine moiety (DiFMU) and one, two, or no methyl groups were added to the D ring (GC240, GC242, and GC486, respectively) (de Saint Germain et al., 2016). In another profluorescent probe, the ABC ring was substituted with the fluorescein moiety (Yoshimulactone green (YLG)) (Tsuchiya et al., 2015) (Supplemental Figure 1B). With the exception of DiFMU, all profluorescent probes stimulated *P. ramosa* germination, although their EC_{50} values were still 1000- to 10 000-fold lower than those of (±)-GR24 (Supplemental Figure 8A–8C, Supplemental Table 2).

Together, these results demonstrate that the stereochemistry of GR24 analogs is crucial for their bioactivity and determines the sensitivity of *P. ramosa* toward these germination-inducing substances. The sensitivity of *P. ramosa* toward desmethyl and 3′-methyl D ring derivatives highlights differences between it and other vascular plants, particularly with regard to signaling via D14 for shoot branching. In addition, the relative bioactivity of the profluorescent SL probes in the stimulation of broomrape germination confirms that ABC rings are not required for bioactivity (Boyer et al., 2014).

SL analogs and mimics interact with PrKAI2d3 according to their germination stimulation activity

The previous results led us to ask whether PrKAI2d3 has the ability to perceive such a large range of structurally divergent compounds and whether its interaction with these molecules is affected by mutations in the catalytic triad. We therefore expressed and purified the PrKAI2d3 and PrKAI2d3^{S98A} proteins *in vitro* and assessed their ability to interact with SLs and other chemical mediators.

Interactions of PrKAI2d3 with SL analogs and profluorescent SL probes were analyzed with nano differential scanning fluorimetry (nanoDSF) by recording changes in tryptophan fluorescence (350 nm/330 nm ratio). In contrast to classic differential scanning fluorimetry (DSF) (Hamiaux et al., 2012), nanoDSF does not require a dye and highlights interactions that do not induce conformational changes. Analysis of the initial fluorescence ratios revealed that the four GR24 stereoisomers interacted with PrKAI2d3 according to their bioactivity (Figure 2D). However, only (+)-GR24 and (−)-2′-*epi*-GR24, the most bioactive analogs with natural configurations, induced an 8.5°C decrease in the PrKAI2d3 melting temperature (Figure 2E), consistent with ligand-mediated protein destabilization.

When GR24 analogs with various methyl groups on their D rings were used, all the analogs interacted with and destabilized PrKAI2d3, although their efficiencies were lower than that of (±)-GR24 and especially that of (±)-3′-Me-GR24 (Figure 2F and 2G). Similar shifts in melting temperatures of the PrKAI2d3 protein were observed with DSF, but without destabilization of the mutated PrKAI2d3^{S98A} protein (Supplemental Figure 9). The bioactive profluorescent probe GC242, used as a racemic mixture or as separate pure enantiomers, also induced a shift in the PrKAI2d3 protein melting temperature (Supplemental Figure 8D–8I). These results suggest that enzymatic activity through Ser98 is required to destabilize the protein.

Next, we estimated PrKAI2d3 affinity for GR24 analogs using a tryptophan intrinsic fluorescence assay. Its affinity was higher for (+)-GR24 and (−)-2′-*epi*-GR24 (K_D = 12.57 ± 2.85 μM and 66.99 ± 26.94 μM, respectively) than for (−)-GR24 and (+)-2′-*epi*-GR24 (K_D = 696 ± 245 μM and 434 ± 593 μM, respectively), consistent with their bioactivity in *P. ramosa* germination (Figure 2H–2K, Supplemental Figure 10). The lower affinity for (±)-3′-Me-GR24 than for (±)-4′-desmethyl-2′-*epi*-GR24 and (±)-GR24 was consistent with their reduced bioactivity range (Figure 2L). However, the protein affinities were significantly lower (micromolar range) than the observed sensitivity of *P. ramosa* (picomolar range). Because similar patterns have been reported for *S. hermonthica* (Tsuchiya et al., 2015), we tested this apparent contradiction by investigating the enzymatic activity of the PrKAI2d3 protein.

PrKAI2d3 enzymatic activity is associated with SL hypersensitivity

First, we tried to visualize PrKAI2d3 hydrolase activity with a generic substrate, *para*-nitrophenyl acetate (*p*-NPA). Surprisingly, no hydrolytic activity was detected (Supplemental Figure 12), in contrast to that observed for other SL receptors treated with the same probe (de Saint Germain et al., 2016). When PrKAI2d3 was incubated with (+)-GR24 and

n = 3). nd, no hydrolysis detected. The asterisks indicate statistical significance from the PrKAI2d3 protein sample as measured by the Kruskal–Wallis test. ***$p \leq 0.001$ and $p > 0.05$.

(C–E) Enzymatic kinetics for PrKAI2d3, PrKAI2d3^{S98A}, AtD14, and AtKAI2 proteins incubated with (±)-GC486 **(C)**, (±)-GC240 **(D)**, and (±)-GC242 **(E)**. Progress curves during hydrolysis of the probes monitored (λ_{em} 460 nm) at 25°C with the use of 400 nM protein and 20 μM probes. The traces represent one of three replicates, and the experiments were repeated at least twice.

(F–H) Hyperbolic plot of the PrKAI2d3 pre-steady-state kinetics reaction velocity with (±)-GC486 **(F)**, (±)-GC240 **(G)**, and (±)-GC242 **(H)**. The initial velocity was determined with profluorescent probe concentrations from 0.3 μM to 40 μM and with proteins at 400 nM. Error bars represent the SE of three replicates, and the experiments were repeated at least three times.

(I) Kinetics constants of probes toward PrKAI2d3. $K_{1/2}$ and k_{cat} are pre-steady-state kinetics constants for PrKAI2d3 with different profluorescent probes and represent the mean ± SE of three replicates.

(J–O) MS characterization of covalent PrKAI2d3-ligand complexes. On the left, deconvoluted electrospray mass spectra of PrKAI2d3 before and after addition of different ligands: (±)-GR24 (500 μM) and (±)-GC486 (500 μM). Peaks with an asterisk correspond to PrKAI2d3 covalently bound to a ligand (PrKAI2d3-ligand). The mass increments were measured for different PrKAI2d3-ligand complexes: 96.3 Da (±)-GR24 and 82.4 Da (±)-GC486. Ligand-modified amino acids were identified by nanoLC-MS/MS analyses after Glu-C proteolysis. On the right, fragmentation spectra of unmodified and different ligand-modified peptides. Labeled peaks correspond to the b and y fragments of the double-charged precursor ion displayed at the top. The histidine residue modified by different ligands is underlined.

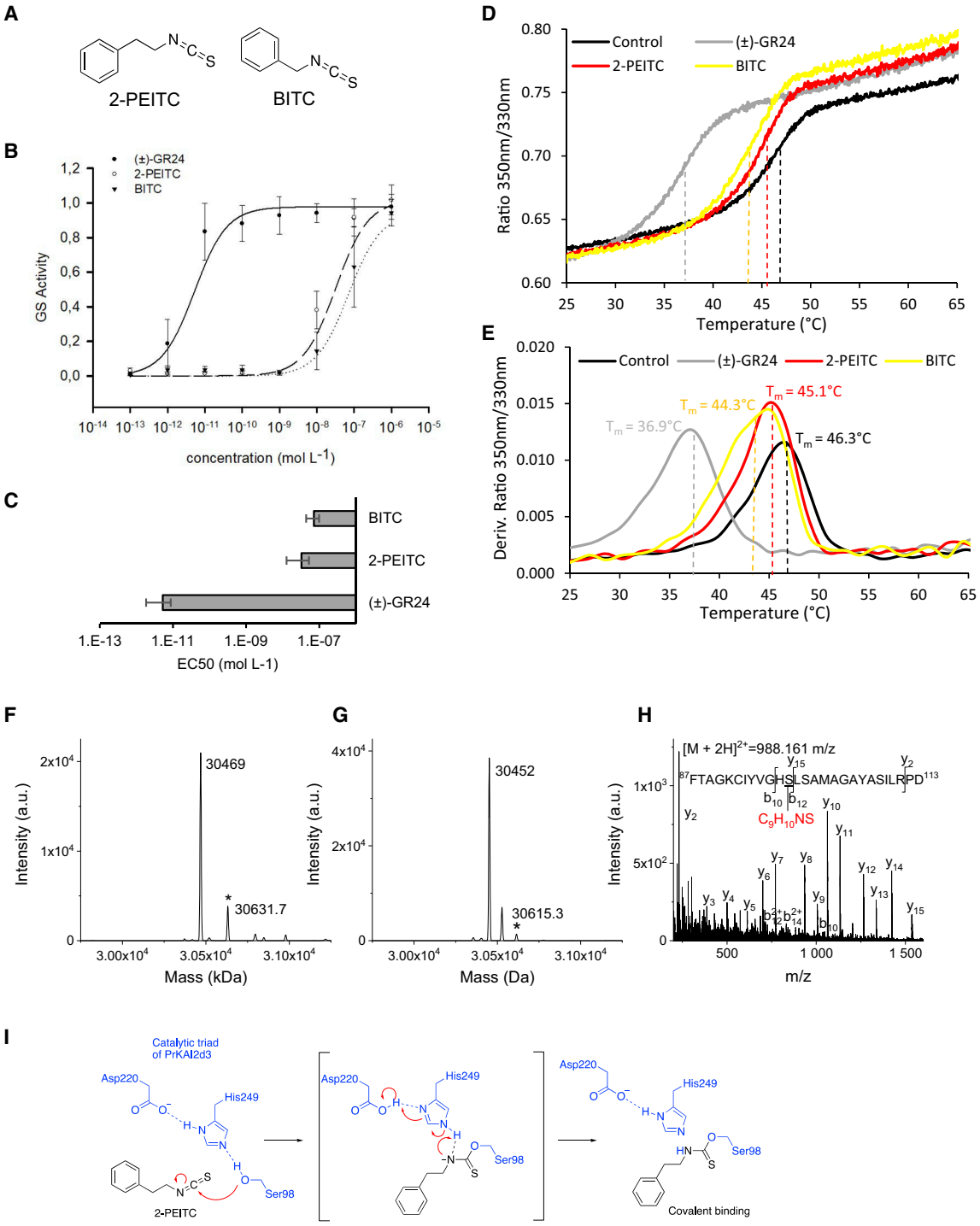

Figure 4. Isothiocyanate germination stimulants are perceived by PrKAI2d3.

(A) Structure of isothiocyanate.

(B and C) Modeled curves of dose-response germination stimulant activities **(B)** and EC_{50} **(C)**. Data are presented ± SE.

(D and E) Thermostability of PrKAI2d3 at 10 μM in the absence of ligand or in the presence of various ligands at 100 μM analyzed by nanoDSF. Changes in fluorescence (F_{350nm}/F_{330nm} ratio) with temperature **(D)** and first derivatives of the F_{350nm}/F_{330nm} curve against the temperature gradient from which the apparent melting temperature (T_m) was determined for each sample **(E)**. The experiment was performed twice.

(F–H) MS characterization of covalent PrKAI2d3-ligand complexes. Deconvoluted electrospray mass spectra of PrKAI2d3 **(F)** and PrKAI2d3^{S98A} **(G)** after addition of the 2-PEITC ligand (1 mM). Peaks with an asterisk correspond to PrKAI2d3 covalently bound to a ligand (PrKAI2d3-ligand). The mass

(legend continued on next page)

(−)-2′-*epi*-GR24, cleavage activity was unambiguously observed by ultraperformance liquid chromatography (UHPLC)/UV diode array detector (DAD) analysis (Figure 3A). However, unlike AtD14 and AtKAI2, PrKAI2d3 did not cleave (−)-GR24 or (+)-2′-*epi*-GR24. Interestingly, a residual cleavage activity of PrKAI2d3^{S98A} still occurred with all GR24 isomers but displayed no stereoselectivity, a result that may explain the partial complementation of *htl-3* with PrKAI2d3^{S98A}-overproducing constructs (Figure 1G). These data suggest that SL hydrolysis and subsequent signal transduction can occur without an intact catalytic triad.

For the interaction assays, we tested the hydrolysis of analogs with substitutions on the D ring. Desmethyl GR24 isomers were more efficiently hydrolyzed than GR24 by AtKAI2, PrKAI2d3, and PrKAI2d3^{S98A} proteins (Figure 3B). In addition, these three purified proteins and AtD14 also displayed low, but significant, hydrolysis activity toward 3′-Me-GR24. These results indicate that PrKAI2d3 possesses an important hydrolysis capacity toward natural configuration-mimicking GR24, albeit to a lesser extent than AtD14.

Enzymatic kinetic characterization of the purified proteins was performed using bioactive profluorescent probes as substrates. Monitoring the DiFMU fluorescence revealed that PrKAI2d3 hydrolyzed (±)-GC240, (±)-GC242, and (±)-GC486 (Figure 3C–3E). For all probes, we observed a biphasic time course of fluorescence, consisting of a burst phase (also called the initial phase) followed by a plateau phase (or a slow phase for AtD14 incubated with (±)-GC240). In all cases, the plateau did not reach the maximum of the expected product (20 μM) but rather a product concentration closer to the protein concentration (0.4 μM) (Figure 3C–3E). This result implied that PrKAI2d3 may act as a single-turnover enzyme toward all GC probes tested, including GC486, which lacks the 3′-methyl group on the D ring and exhibits Michaelian cleavage kinetics with AtD14 and RMS3/PsD14 proteins (de Saint Germain et al., 2016). The S98A substitution in the catalytic triad drastically reduced (±)-GC240 and (±)-GC242 cleavage, although residual activity toward (±)-GC486 remained statistically significant. These observations confirmed that mutation of the catalytic triad does not fully abolish cleavage activity toward a compound without methyl on the D ring.

For single-turnover enzymes, we defined k_{cat} as the rate constant of the pre-steady-state phase (initial phase) and $K_{1/2}$ as the probe concentration with half maximal velocity (V_{max}) (Figure 3G–3I). The similar $K_{1/2}$ values of PrKAI2d3 with (±)-GC240 and (±)-GC242 (5.74 μM and 4.60 μM, respectively) confirmed the minor influence of the C3′ methyl chain on substrate affinity. However, differences in V_{max} (0.072 M.min^{-1} and 0.013 M.min^{-1}, respectively) indicated that the C3′ methyl chain reduces the catalytic activity, consistent with the bioactivities of these probes. Higher $K_{1/2}$ values of PrKAI2d3 for (±)-GC240 than for (±)-GC486 (5.74 μM and 1.53 μM, respectively) and different V_{max} values (0.072 M.min^{-1} and 0.209 M.min^{-1}, respectively) highlighted the importance of the C4′ methyl chain for binding and catalytic affinity, supporting the results of the germination bioassays (Supplemental Figure 8A–8C).

To test the hypothesis that PrKAI2d3 forms a stable intermediate with the D ring, as previously demonstrated for other SL receptors (AtD14, PsD14/RMS3, ShHTL7, and D14) (de Saint Germain et al., 2016; Yao et al., 2016, 2017, 2018b), we incubated two bioactive ligands (±)-GR24 and probe (±)-GC486 with PrKAI2d3 at a pH of 6.8 and recorded mass spectrometry (MS) spectra under denaturing conditions. In all cases, a mass shift occurred corresponding to the D ring covalently bound to the protein (Figure 3J–3L) and specifically attached to His249 of the catalytic triad (Figure 3M–3O).

ITCs interact with PrKAI2d3 and generate a covalent adduct to the catalytic serine

Although PrKAI2d3 perceives structurally diverging SL analogs and mimics that stimulate *P. ramosa* seed germination, the specificity of the interaction between rapeseed and *P. ramosa* correlates with the parasite's ability to perceive ITCs, which differ greatly in structure from SLs (Auger et al., 2012). We therefore evaluated the ability of PrKAI2d3 to perceive ITCs. Seeds of *P. ramosa* were approximately 10 000-fold less sensitive to 2-PEITC and BITC than to (±)-GR24 (Figure 4A–4C). Investigation of the putative interactions between PrKAI2d3 and ITCs by nanoDSF revealed a small shift (1.2°C–2.0°C) in the PrKAI2d3 melting temperature in response to high ITC concentrations, a result that was further confirmed by classic DSF (Figure 4D and 4E, Supplemental Figure 13). These data indicated that ITCs interact with PrKAI2d3 with low affinity, corresponding with a stimulating potential on *P. ramosa* seeds lower than that of bioactive SLs (Auger et al., 2012) and their analogs. Finally, the apparent melting temperatures of PrKAI2d3 with BITC and 2-PEITC (44.3°C and 45.1°C, respectively) varied from those obtained with (±)-GR24 (36.9°C), suggesting that ITCs may induce a conformational change that differs from GR24-induced destabilization.

Because ITCs react easily with nucleophile functions (Satchell et al., 1990), we hypothesized that the interaction of PrKAI2d3 with ITCs may trigger the formation of a covalent adduct. Indeed, a mass shift was detected that correlated with the covalent binding of 2-PEITC to the protein (Figure 4F). After digestion of the PrKAI2d3-2-PEITC complex, the 2-PEITC attachment was localized to a peptide that corresponded to amino acids 87–113 of PrKAI2d3. Tandem MS (MS/MS) data revealed that the 2-PEITC attachment could be on His97 or on the catalytic Ser98 (Figure 4H). Incubation of 2-PEITC with PrKAI2d3^{S98A} allowed us to conclude that Ser98 is the major site for 2-PEITC attachment (Figure 4G). These results hint at a perception mechanism for ITC in which the Ser98 hydroxyl group reacts with isothiocyanate to generate a PrKAI2d3-attached carbamothioate (Figure 4I). However, no 2-PEITC attachment was detected on His249-containing peptides of the catalytic triad.

increments were measured for the PrKAI2d3-2-PEITC complex, 162.7 Da. Ligand-modified amino acids were identified by nanoLC-MS/MS analyses after Glu-C proteolysis. **(H)** Fragmentation spectra of unmodified and different ligand-modified peptides. Labeled peaks correspond to the b and y fragments of the double-charged precursor ion displayed at the top. The PEITC ligand-modified serine residue is underlined.

(I) Perception mechanism of PEITC.

Finally, it is noteworthy that the germination of *Arabidopsis* Col-0, *htl-3*, and the three p35S::GFP-PrKAI2d3 complemented lines was insensitive to 2-PEITC (data not shown).

Overall, PrKAI2d3 acts as a receptor for both SL-like molecules and ITCs, both of which are germination stimulants for *P. ramosa*. These results demonstrate that further research into potential chemical interactors is achievable and may enable the design of control methods.

The search for small-molecule interactors of PrKAI2d3 identified D-OH as a simple and efficient germination stimulant for *P. ramosa* with a bioactivity similar to that of ITCs

Recently, synthetic inhibitors of D14 and ShHTL7 (the best-characterized SL receptor in *S. hermonthica*) (Waters, 2019) have been proposed. These include soporidine, KK094, Triton X, and tolfenamic acid (TA) (Figure 5A), all of which are structurally unrelated to SLs. We evaluated the putative inhibitory effects of these compounds, as well as those of the common serine protease inhibitor phenylmethylsulfonyl fluoride (PMSF), on the germination of *P. ramosa* seeds treated with 10 nM (±)-GR24 or 100 nM 2-PEITC. *P. ramosa* seeds were clearly hyposensitive to each of these compounds compared with the results obtained in *S. hermonthica*, and maximum inhibition was obtained at very high concentrations in some instances (Figure 5B and 5C; Supplemental Table 3). Indeed, all half maximum inhibitory concentrations (IC_{50}) fell above the IC_{50} of abscisic acid (ABA; 100 nM [GR24] and 34 nM [2-PEITC]), a known inhibitor of *P. ramosa* germination (Zehhar et al., 2002; Lechat et al., 2015). These data indicate that the use of germination inhibitors intended for *Striga* is relatively irrelevant and unsuitable for *P. ramosa* biological control.

We therefore looked for specific PrKAI2d3 agonists with the potential for large-scale biocontrol. A serious issue in the search for simple and inexpensive SL analogs and mimics is their low stability owing to the connection of the D ring to a leaving group. As alternatives, molecules have been proposed that carry the D ring only, as it is essential for the high bioactivity of SLs (Takahashi and Asami, 2018). We specifically evaluated the effect of a set of butenolides that contained the D ring (D-OR) only on *P. ramosa* germination (Figure 5D–5F, Supplemental Figure 14). D-O*sec*Bu and 3′-Me-D-OH were completely inactive, and the *P. ramosa* sensitivity toward D-OAll, D-OMe, D-OEt, and dihydro-DOEt was low, with EC_{50} values in the micromolar range. By contrast, 4-Hydroxy-2-methylbut-2-en-4-olide (D-OH) and 4′-desmethyl-D-OH were approximately 10-fold more active than 2-PEITC (Supplemental Table 2). Although D-OH is bioactive in rice (*Oryza sativa*) at a high concentration (50 μM) (Nakamura et al., 2013), direct injection of D-OH and 3′-Me-D-OH (100 μM) in the stem had no effect on branching control in pea (Supplemental Figure 15).

To determine whether D-OH sensitivity was specific to *P. ramosa* PrKAI2d3, we reexamined the germination-stimulating activity of D-OH on *S. hermonthica*. In contrast to previous results (Johnson et al., 1976; Pepperman et al., 1982), D-OH induced *S. hermonthica* germination (EC_{50} = 1.2 μM). Moreover, in *Arabidopsis* lines expressing GFP fused to ShHTL7, the known *S. hermonthica* SL receptor (Tsuchiya et al., 2015; Xu et al., 2018) was induced by (±)-DOH (EC_{50} = 3.1 μM) (Supplemental Figure 16, Supplemental Table 1). In summary, our study confirms the perception of D-OH by SL receptors in root-parasitic plants.

DSF and intrinsic fluorescence analyses revealed that D-OH and PrKAI2d3 interacted at high concentrations (Figure 5G and 5H). Incubation of D-OH with PrKAI2d3 at pH 6.8 and MS spectra recorded under denaturing conditions revealed a mass shift corresponding to the covalent binding of the D ring to the protein (Figure 5I). The D-ring attachment could be localized to His249 of the catalytic triad, similar to that observed for the SL analogs (Figure 5J). The observed shift of 114.2 Da (Figure 5I), contrasting with the shift of 96.3 Da observed with (±)-GR24 (Figure 3K), led us to propose a mechanism of complex formation (Supplemental Figure 14F). In this hypothetical mechanism, His247 directly attacks the α,β unsaturated system in D-OH. Unlike the interaction with GR24, this mechanism would not implicate the action of Ser98 because the complex is observed with the mutant protein $PrKAI2d3^{S98A}$ (Supplemental Figure 14E). The ability of PrKAI2d3 to interact with D-OH—as well as various SL analogs, SL-like compounds, and ITCs—highlights the plasticity that permits it to exert significant biological activity through interaction with different structures and emphasizes that all SL hydrolysis products can act as germination stimulants of *P. ramosa.*

DISCUSSION

Obligate parasitic weeds require host-derived signals to germinate and wither their hosts long before they emerge from the soil, arguably making the early stages of the parasitic life cycle a much better target for control strategies than the later stages (Vurro et al., 2016). An important prerequisite for the design of such methods is an in-depth understanding of how parasites perceive germination stimulants.

In this study, we identified five *KAI2* genes in the parasitic plant species *P. ramosa*. However, we acknowledge that this is arguably an underestimate, as these sequences were obtained from the *P. ramosa* reference transcriptome (Goyet et al., 2017). It is now necessary to search exhaustively for all *KAI2* genes in the forthcoming genomic sequences, which will also help to refine the KAI2 phylogeny in this species and within the *Orobanchaceae* family (Bythell-Douglas et al., 2017; Conn et al., 2015). We demonstrated that PrKAI2d3 provides *P. ramosa* with hypersensitivity to rhizosphere SLs, mainly due to its enzymatic activity. Enzymatic data with GR24 analogs [(+)-GR24 and (−)-2′-*epi*-GR24] and GC probes suggest that PrKAI2d3 acts as a single-turnover enzyme toward profluorescent probes and SL analogs. PrKAI2d3 cleaves these probes and analogs to form a covalent complex between the D ring and the catalytic histidine, as previously described for AtD14 and RMS3, the receptors of SL as a hormonal signal (de Saint Germain et al., 2016). However, this model has recently been challenged (Seto et al., 2019) by the finding that an AtD14 mutant for the catalytic Asp residue can transduce the SL signal, although it is unable to cleave endogenous SL. Hence, it has been concluded that SL cleavage is not required for hormonal SL signaling. Indeed, it is possible that certain SL analogs can be perceived independently

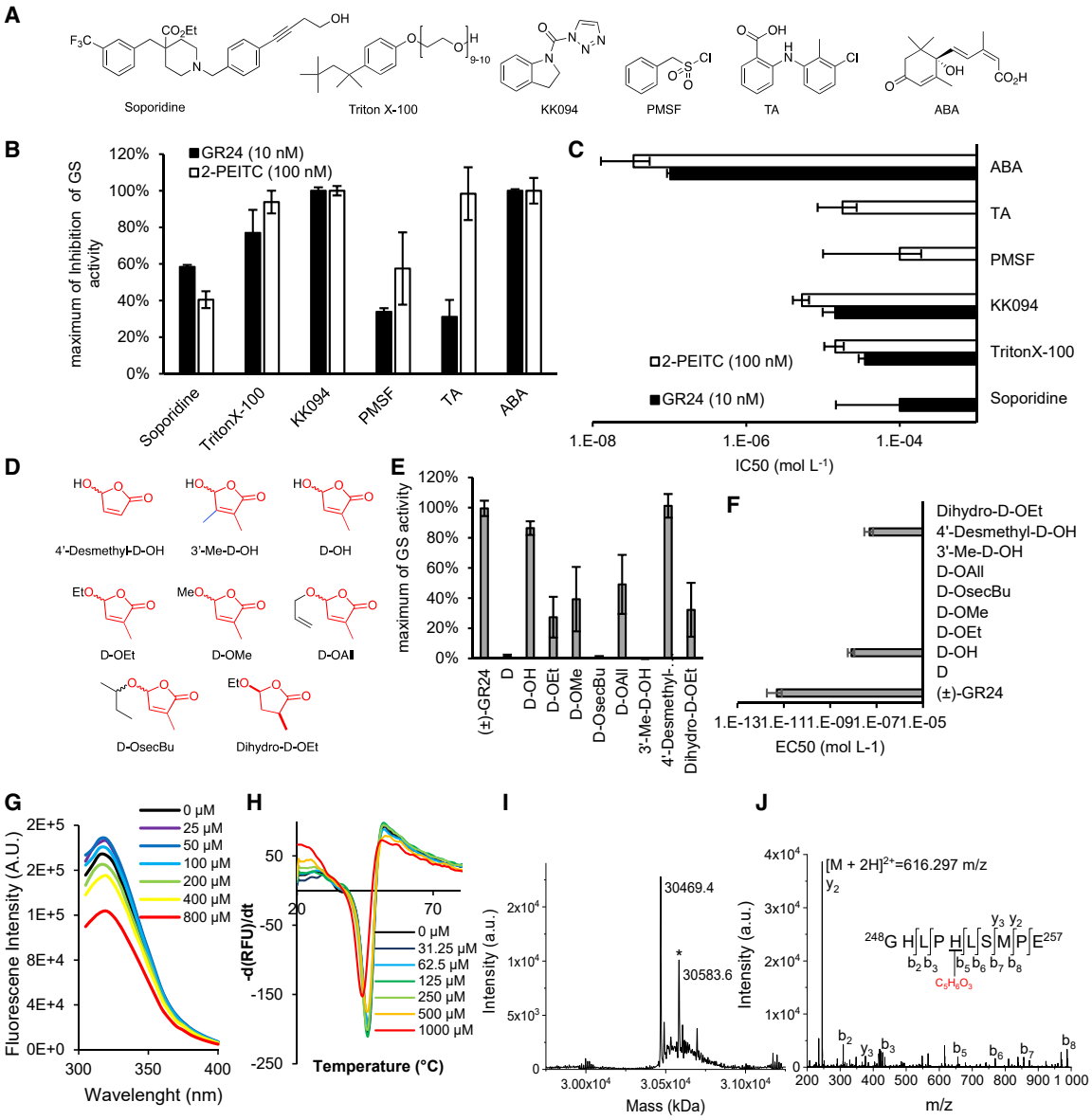

Figure 5. Identification of antagonists and agonists for *P. ramosa* seed germination.

(A) Chemical structures of inhibitors of D14 protein and ABA.

(B and C) Comparison of the inhibitory effect on *P. ramosa* germination stimulation (GS) induced by GR24 (10 nM) or 2-PEITC (100 nM). Maximum inhibition **(B)** and IC_{50} **(C)**.

(D) Structure of D-OH rings and derivatives.

(E and F) GS activity of D-OH and its derivatives on *P. ramosa* seeds. Maximum GS activity **(E)** and EC_{50} **(F)**.

(G) D-OH binding of PrKAI2d3, based on intrinsic tryptophan fluorescence. Plots of fluorescence intensity versus probe concentrations. The change in intrinsic fluorescence was monitored and used to determine the apparent K_D values. The plots represent the mean of two replicates, and the experiments were repeated at least three times. The analysis was performed with GraphPad Prism 7.05 software.

(H) Biochemical analysis of the interaction between PrKAI2d3 at 10 μM and D-OH at various concentrations by DSF. Each line represents the average protein melt curve for two technical replicates, and the experiment was performed twice.

(I and J) MS characterization of covalent PrKAI2d3-D-OH complexes. **(I)** Deconvoluted electrospray mass spectrum of PrKAI2d3 after addition of the D-OH ligand (5 mM). Peaks with an asterisk correspond to PrKAI2d3 covalently bound to D-OH. The mass increments were measured for the PrKAI2d3-D-OH complex, 114.2 Da. Ligand-modified amino acids were identified by nanoLC-MS/MS analyses after Glu-C proteolysis. **(J)** Fragmentation spectra of unmodified and different ligand-modified peptides. Labeled peaks correspond to the b and y fragments of the double-charged precursor ion displayed at the top. The D-OH ligand-modified histidine residue is underlined.

of enzymatic activity. We showed that GR24 analogs with non-natural stereochemistry [(−)-GR24 and (+)-2′-*epi*-GR24] are not cleaved by PrKAI2d3. These uncleaved molecules stimulate *P. ramosa* seed germination 100-fold less efficiently than GR24 stereoisomers with a natural stereochemistry (Figure 3). Moreover, the affinity (K_D) of PrKAI2d3 toward the most bioactive

SL analogs, (+)-GR24 and (−)-2′-*epi*-GR24, is in the micromolar range, several orders lower than the *P. ramosa* seed sensitivity recorded in the germination bioassays. The K_D values for (+)-GR24 and (−)-2′-*epi*-GR24, which reflect simple binding to the receptor, do not explain this hypersensitivity. Similar differences between *in vitro* and *in vivo* analyses were observed for the *S. hermonthica* SL receptor ShHTL7 (Tsuchiya et al., 2015). Like *Striga, P. ramosa* may use a similar mechanism of SL perception based on recognition by the active binding pocket, as observed in D14 and its orthologs. However, the hypersensitivity of root-parasitic plants for SLs is unique and could suggest different mechanisms for the perception of hormonal and rhizospheric SLs. Nevertheless, we propose that the SL hypersensitivity of this SL receptor is due to its enzymatic properties, as previously proposed for the femtomolar-range germination stimulant sphynolactone-7 (Uraguchi et al., 2018), which is also aSL mimic.

Interestingly, enzymatic activity is not completely abolished in the PrKAI2d3^{S98A} protein. Significant residual activity is also present in the DAD2^{S96A} protein (Lee et al., 2020). The characterization of a serine protease enzyme in the 1980s demonstrated that the substitution of a catalytic residue by an alanine does not fully abolish enzyme activity (Carter and Wells, 1988). This observation could explain the partial complementation of the *htl-3* mutant with constructs that overproduce PrKAI2d3^{S98A}. A similar proposition could also explain why *Arabidopsis* that overexpress AtD14 with a mutated Asp catalytic residue is able to transduce a branching inhibitor signal, especially the still-untested natural SLs present in *Arabidopsis* (i.e., non-canonical SLs). However, the His covalent adduct was not detected after incubation of (±)-GR24 with the PrKAI2d3^{S98A} protein (Supplemental Figure 14F), which could also suggest that both enzyme activity and His modification are not critical for SL signal transduction. Notably, *p*-NPA did not efficiently demonstrate the enzymatic activity of PrKAI2d3 compared with profluorescent SL mimics, pinpointing the weakness of using generic or inappropriate substrates as controls.

Moreover, PrKAI2d3 displays high plasticity that allows it to bind modified SLs such as desmethyl-GR24 isomers or many SL mimics, but in contrast to RMS3 and AtD14, it perceives these compounds similarly to intact SLs. Likewise, desmethyl-YLG was bioactive in *Arabidopsis* via AtKAI2 (Yao et al., 2018a). Ligand-mediated protein destabilization is not required to perceive SL analogs, but it considerably improves the sensitivity to natural SLs. PrKAI2d3 acts as a single-turnover enzyme for compounds with a D ring that lack a methyl group at the C4′ position, but a methyl group at the C-3′ position led to low interaction with PrKAI2d3. This result is consistent with the low *P. ramosa* germination stimulation activity of 3′-methyl analogs and mimics, and it corroborates studies conducted in *Orobanche cumana*, *Orobanche minor*, *P. aegyptiaca*, and *S. hermonthica* (Boyer et al., 2014; Jamil et al., 2019). In other words, *P. ramosa* may be sensitive to D-ring-modified SL and may perceive diverse SL-related compounds as putative SL degradation products (Yamauchi et al., 2018).

In addition, we established that ITCs, other known germination stimulants, interact with the PrKAI2d3 protein by forming a covalent complex. In *P. ramosa*, PrKAI2d3 can be considered a germination stimulant receptor for different chemicals, including SLs, SL derivatives and mimics, and also ITCs with completely different structures. Thus, *P. ramosa* has seemingly optimized its germination capacity by enhancing its ability to perceive various chemical mediators emitted by host plants. The enzymatic activity-dependent ITC perception mechanism suggests that the active catalytic triad may have been conserved to perceive not only SLs but also other germination stimulants that are not yet characterized for *P. ramosa*. On the other hand, 2-PEITC does not trigger *Arabidopsis* seed germination, even when complemented with PrKAI2d3. This suggests that *Arabidopsis* does not possess the necessary machinery for the perception or transduction of ITC signals.

SLs are very unstable in the soil, especially under basic conditions that produce ABC=CHOH and D-OH derivatives. To date, all SL analogs and mimics possess a D ring connected to an ABC mimic by a hydrolysable function. SL agonist treatments developed to date induce the suicide germination of parasitic plant seeds (Zwanenburg and Pospíšil, 2013). Nevertheless, these agonists are too unstable to be effective under field conditions, even when promising chemicals are designed and applied for *S. hermonthica* (Uraguchi et al., 2018). In addition, cultures of *P. ramosa*-infested rapeseed occur mainly in slightly basic soils (Johnson et al., 1981), favoring the formation of ITCs (Auger et al., 2012) and complicating the use of SL mimics as a suicidal germination strategy, especially because of their instability. In sharp contrast, *P. ramosa* is highly sensitive to D-OH or DesMe-D-OH. As for D-H, no germination activity was detected, and the hemiacetal function seems very important for the interaction with PrKAI2d3. Moreover, the residual bioactivity of D-OR ($R \neq H$) may be explained by the hydrolysis of the R group during the bioassay, leading to D-OH. D-OH and DesMe-D-OH are especially interesting for translational research, because both compounds are small, easily synthesized compared to synthetic SLs and SL mimics, and not subject to rapid degradation. As such, D-OH and DesMe-D-OH seem to be promising chemicals for suicide germination in the field; higher active concentrations can compensate for their lower germination activity compared with SL mimics. Moreover, D-OH has the great advantage of being a natural product. The use of SL mimics, in which the portion equivalent to the ABC moiety is typically xenobiotic, increases the risk of potential toxicity or environmental pollution. In contrast to previous studies (Johnson et al., 1976; Pepperman et al., 1982), we found that D-OH is bioactive as a witchweed seed germination stimulant and that it could possibly be used for *S. hermonthica* biocontrol.

Here, we identified germination inhibitors and demonstrated the involvement of α/β-hydrolases in germination stimulant perception, providing an alternative approach for fighting *P. ramosa* (Yoneyama, 2016). Novel, more active inhibitors must be designed to control *P. ramosa* infection without negative effects on host plants and arbuscular mycorrhizal fungi. For this purpose, the identification of the SL receptor(s) in these fungi will undoubtedly be an important milestone. The use of specific inhibitors should be combined with other approaches for integrated management strategies (Pickett et al., 1997), such as chemical suicidal germination with compounds such as D-OH to decrease the parasitic plant seed bank in the soil.

METHODS

Preparation of GR24 isomers, probes, and other ligands

See Supplemental methods.

Expression and purification

AtD14 and AtKAI2 were purified and expressed with cleavable GST tags as described previously (de Saint Germain et al., 2016). For PrKAI2d3 expression, the coding sequences from *P. ramosa* were amplified by PCR using a seed-derived cDNA template and specific primers (Supplemental Table 4) containing a protease cleavage site for tag removal and were subsequently cloned into the pGEXT-4T-3 expression vector. The PrKAI2d3 and PrKAI2d3^{S98A} proteins were purified and expressed as described above.

Site-directed mutagenesis

Site-directed mutagenesis experiments were performed on pGEX-4T-3-PrKAI2d3 (Supplemental Table 4) using the QuikChange II XL Site-Directed Mutagenesis Kit (Stratagene). Mutagenesis was verified by systematic DNA sequencing.

Plant materials and growth conditions

For pea (*P. sativum*) and *A. thaliana*, see Supplemental methods.

Two batches of parasitic plant seeds were used. A population of *P. ramosa* (L.) Pomel seeds associated with genetic group 1 (*P. ramosa* 1) was collected in Saint-Martin-de-Fraigneau (France) from broomrape-parasitized winter rapeseed (*Brassica napus* L.) in 2014 and 2015 (Stojanova et al., 2019). Seeds of *S. hermonthica* (Delile) Benth. (Sudan, 2007) were provided by Lukas Spichal (Olomouc, Czech Republic). Seeds were surface sterilized and conditioned as described previously (Pouvreau et al., 2013) (darkness; 21°C for *P. ramosa* and 30°C for *S. hermonthica*).

Pea shoot branching assay

See Supplemental methods.

Cloning and generation of transgenic lines

For all GFP fusion constructs, cloning was performed by Gateway recombination (Thermo Fisher Scientific). The open reading frame (ORF) of PrKAI2d3 was amplified from *P. ramosa* cDNA with iProof High-Fidelity DNA Polymerase (Bio-Rad) and the Gateway-specific primers PrKAI2d3_B2_FW and PrKAI2d3_B3_Rev_STOP. The PCR product flanked by attB sites was cloned into pDONR P2R-P3 using BP Clonase II enzyme mix (Invitrogen). The resulting entry vector was used to clone the genes into the destination vector pK7m34GW under the control of the 35S promoter and N-terminally fused with GFP using LR Clonase II Plus enzyme mix (Invitrogen). To construct the catalytic site mutant, pDONR P2R-P3-PrKAI2d3 was mutated with the QuikChange II Site-Directed Mutagenesis Kit (Agilent). The generated clones were checked by sequencing. All primers used for cloning are listed in Supplemental Table 4.

Western blotting

Total protein was extracted from 5-day-old seedlings that had been exposed to white light for 3 h, transferred to darkness for 21 h, and exposed to continuous red light for 4 days. Protein concentrations were determined by the Bradford assay (Bio-Rad). Thirty micrograms of protein extract were separated by SDS-PAGE, transferred onto polyvinylidene fluoride (PVDF) membranes, and treated with horseradish peroxidase (HRP)-conjugated antibodies against GFP (anti-GFP-HRP, 1:10 000, Miltenyi Biotec) or anti-tubulin (mouse monoclonal, 1:10 000, Sigma-Aldrich) and HRP-conjugated anti-mouse antibodies (rabbit polyclonal, 1:10 000, Abcam). The blots were visualized using the Western Lightning Plus Enhanced Chemiluminescence kit (PerkinElmer) and the X-Doc System (Bio-Rad). Precision Plus Protein Dual Color Standards (Bio-Rad) were used as protein size markers.

Arabidopsis *hypocotyl elongation assays*

Arabidopsis seeds were surface sterilized by consecutive treatments of 70% (v/v) ethanol with 0.05% (w/v) SDS for 5 min and 95% (v/v) ethanol for 5 min, then sown on half-strength Murashige and Skoog medium (Duchefa Biochemie) containing 1% (w/v) agar and supplemented with 1 μM (±)-GR24 (0.01% [v/v] DMSO) or 0.01% (v/v) DMSO only (control). Seeds were stratified at 4°C for 2 days in the dark, exposed to white light for 3 h, transferred to darkness for 21 h, and exposed to continuous red light for 4 days at 21°C. Plates were photographed, and hypocotyl lengths were quantified using ImageJ (http://imagej.nih.gov/ij/).

Arabidopsis *germination assays*

Arabidopsis seeds were after-ripened for at least 6 weeks before use. Surface-sterilized seeds were incubated in incubation solution (1 mM HEPES buffer; pH 7.5) at a ratio of 10 mg of seeds per milliliter (Lechat et al., 2015). Fifty microliters of seeds (~20–25 seeds) were distributed on 96-well plates, and 10 μL of germination stimulant [10 μM (+)-GR24, 10 μM (−)-GR24, and 0.1% (v/v) DMSO (control) or 10-fold concentrated D-OH] were added. The final volume was adjusted to 100 μL with incubation solution. Plates were incubated for either 5 days at 25°C in the dark (Brun et al., 2019) or 7 days at 32°C–34°C under constant illumination at a quantum irradiance of 10 μmol m^{-2} s^{-1} (Toh et al., 2012; Toh et al., 2015). A seed was considered to have germinated when the radicle protruded from the seed coat.

Germination stimulation activity assay on the seeds of root-parasitic plants

The germination stimulation activity of chemicals on the seeds of parasitic plants was determined as described previously (Pouvreau et al., 2013). Chemicals were suspended in DMSO at 10 mmol L^{-1}, diluted with water to 1 mmol L^{-1} (water/DMSO; v/v; 9:1), and further diluted from 1 × 10^{-5} mol L^{-1} to 1 × 10^{-12} mol L^{-1} with water/DMSO (v/v; 9:1). Each compound was applied to conditioned parasitic seeds at a concentration range from 10^{-13} to 10^{-6} mol L^{-1} (water/DMSO; 99:1). One percent (v/v) DMSO was used as a negative control (seed germination <1%), and 1 μmol L^{-1} (±)-GR24 was used as a positive control (seed germination 72%–87% and 50%–65% for *P. ramosa* 1 and *S. hermonthica*, respectively). To avoid variation related to sterilization events, germination percentages are reported as a ratio relative to the positive control (1 μmol L^{-1} [±]-GR24) included in each germination assay. Each dilution and germination assay was repeated at least three times. For each compound tested, dose-response curves (germination stimulation activity = f(c); germination stimulant activity relative to 1 μmol L^{-1} (±)-GR24; c, concentration (mol L^{-1})); EC_{50}; and maximum germination stimulant activity) were determined with a four-parameter logistic curve computed with SigmaPlot 10.0.

Enzymatic degradation of GR24 isomers by purified proteins

See Supplemental methods.

Enzymatic assays with profluorescent probes and p*-nitrophenyl acetate*

These assays were performed as described previously (de Saint Germain et al., 2016) using a TriStar LB 941 Multimode Microplate Reader (Berthold Technologies).

Protein melting temperatures

For DSF, see Supplemental methods.

nanoDSF

Proteins were diluted in PBS (100 mM phosphate, pH 6.8, 150 mM NaCl) to a concentration of ~10 μM. Ligands were tested at a concentration of 200 μM. The intrinsic fluorescence signal was measured as a function of increasing temperature using a Prometheus NT.48 fluorimeter (NanoTemper Technologies) with 55% excitation light intensity and a 1°C/min temperature ramp. Analyses were performed on capillaries filled with 10 μL of the respective samples. Intrinsic fluorescence signals expressed by the 350 nm:330 nm emission ratio, which increases as proteins unfold, were plotted as a function of temperature (Figures 2D, 2F, and 4D). The plots show one of three independent data collections performed for each protein.

Intrinsic tryptophan fluorescence assays and determination of the dissociation constant K_D

These experiments were performed as described previously (de Saint Germain et al., 2016) using a Spark Multimode Microplate Reader (Tecan).

Direct electrospray ionization MS under denaturing conditions and localization of the fixation site of ligands on PrKAI2d3

See Supplemental methods.

Phylogenetic analyses

Phylogenetic analyses were performed on 32 D14 and KAI2 sequences, including five *P. ramosa* sequences obtained in the present study, as well as previously described sequences from *P. aegyptiaca*, *S. hermonthica*, *P. sativum*, *A. thaliana*, and *O. sativa* (Arite et al., 2009; Waters et al., 2012; Conn et al., 2015; Toh et al., 2015; de Saint Germain et al., 2016; Carbonnel et al., 2019). The D14 and KAI2 proteins and nucleotide sequences (Supplemental Data 1 and 2, respectively) were aligned using MAFFT (multiple alignment using fast Fourier transform) (Katoh et al., 2019) with the G-INS-i iterative refinement alignment method (Katoh et al., 2005). Sequence alignments (Supplemental Data 3 and 4) were manually trimmed to remove gaps at either end, producing final protein and nucleotide data sets of 262–264 amino acids and 786–792 nucleotides, respectively (Supplemental Data 5 and 6). The α/β hydrolase RbsQ from *Bacillus subtilis* was used as an outgroup because of its high similarity to KAI2 and D14 and its possession of a conserved catalytic triad (Waters et al., 2012). ML analyses were performed in RAxML (Stamatakis, 2014) with 1000 bootstrap replicates. The best ML tree for the amino acid sequences was inferred with the PROT-GAMMA model and the WAG substitution matrix, and the best ML tree for the nucleotide sequences was inferred with the general time reversible (GTR) model with the gamma rate of heterogeneity among sites. The percentage of trees in which the associated taxa clustered together was indicated next to the branches. The resulting consensus amino acid and nucleotide trees were drawn to scale using MEGA7 (Kumar et al., 2016) with branch lengths representing the number of substitutions per site.

Modeling

P. ramosa KAI2 protein sequences were modeled using the SWISS-MODEL server (http://swissmodel.expasy.org/) (Waterhouse et al., 2018). Models were generated using chain A of the Apo form of the *Arabidopsis* KAI2 structure (PDB: 4JYP) as a template (Guo et al., 2013). Protein structure figures were generated with PyMOL, and cavities within homology models were visualized using surface mode on the setting "cavities and pockets culled." Pocket sizes were calculated using the CASTp 3.0 server (Tian et al., 2018) with a probe radius of 1.4 Å. The reported pocket sizes were the Connolly solvent excluded surface volumes of the catalytic pocket.

Expression data

Seeds of *A. thaliana* complemented lines were imbibed for 24 h in a growth solution (1 mM HEPES buffer, pH 7.5, 0.1 mM Preservative Plant Mixture in sterile water) and treated for 6 h with 10 μM (±)-GR24 or a mock solution. Seeds were dried using a paper tissue, snap-frozen in liquid nitrogen, and ground to a fine powder with a mortar and pestle. RNA was extracted and purified with the RNeasy Plant Mini Kit (Qiagen). Genomic DNA was removed by DNase treatment, and the samples were purified by ammonium acetate (5 M final concentration) precipitation. The iScript cDNA Synthesis Kit (Bio-Rad) was used to reverse transcribe RNA. SYBR Green detection was used for qRT-PCR on a Light Cycler 480 system (Roche). Reactions were performed in triplicate on a 384-well plate in a total volume of 5 μL with a cDNA fraction of 10%. Seeds of *P. ramosa* were imbibed in the growth solution (see above) for 7 days, then treated for 6 h with 0.1 μM (±)-GR24, 0.1 μM 2-PEITC, or a mock solution. Seeds were dried using a paper tissue, snap-frozen in liquid nitrogen, and ground to a fine powder with a mortar and pestle. RNA was extracted and purified with the PureLink RNA Mini Kit (Invitrogen). Genomic DNA was removed by DNase treatment, and the samples were purified using the RNeasy PowerClean Pro CleanUp Kit (Qiagen). Three hundred nanograms of total RNA were reverse transcribed using the High-Capacity cDNA Reverse Transcription Kit (Applied Biosystems). SYBR Green detection was used for qRT-PCR on a CFX Connect Real-Time PCR Detection System (Bio-Rad). Reactions were performed in triplicate on a 96-well plate in a total volume of 20 μL with a cDNA fraction of 25%. Cycle threshold values were obtained and analyzed by the $2^{-\Delta\Delta CT}$ method (Livak and Schmittgen, 2001). For *A. thaliana*, the values from three biological replicates and three technical replicates were normalized against those of the seed-specific housekeeping gene At4g12590 (Dekkers et al., 2011). For *P. ramosa*, the values from three biological replicates and two technical replicates were normalized against those of the *EF1-α* gene (Lechat et al., 2012). The normalized values were analyzed according to a published model (Rasmussen et al., 2012) using the mixed model procedure (SAS Enterprise).

Statistical analyses

Because deviations from normality have been observed for axillary bud length, hypocotyl length, and germination after SL treatments, the Kruskal–Wallis test was used to test for significant differences between treatment with one compound and treatment with another using R Commander software (version 1.7–3) (Fox, 2016).

SUPPLEMENTAL INFORMATION

Supplemental information is available at *Plant Communications Online*.

FUNDING

This work was supported by the Institut Jean-Pierre Bourgin's Plant Observatory technological platforms and has benefited from the facilities and expertise of the I2BC proteomic platform (Proteomic-Gif, SICaPS) supported by Infrastructures en Biologie Santé et Agronomie, Ile de France Region, Plan Cancer, CNRS, and Paris-Sud University. The CHARM3AT Labex program (ANR-11-LABX-39) is also acknowledged for its support. A.d.S.G. is the recipient of an AgreenSkills award from the European Union in the framework of the Marie-Curie FP7 COFUND People Program and a fellowship from Saclay Plant Sciences (ANR-17-EUR-0007). A.J. is indebted to the Research Foundation Flanders for a Structural Basic Research fellowship (project 1S15817N) and for a travel grant in the framework of a Tournesol fellowship (project VS04418N).

AUTHOR CONTRIBUTIONS

A.d.S.G., J.-B.P., and F.-D.B. designed the research. G.C. designed and synthesized the profluorescent probes. V.Se. and F.-D.B. synthesized the chemicals. A.d.S.G., A.J., and E.B. produced and purified the proteins. A.d.S.G. and A.J. characterized the proteins and performed the kinetic experiments. A.J., G.B., J.-B.P., and F.-D.B. performed the plant experiments. D.C. performed the mass spectrometry experiments. A.d.S.G., V.St., and F.-D.B. performed the high-pressure liquid chromatography analyses and separations. A.d.S.G., A.J., G.B., J.-B.P., L.B., D.C., K.G., P.S., S.W., S.G., P.D., and F.-D.B. analyzed the data. A.d.S.G., A.J., G.B., J.-B.P., and F.-D.B. wrote the paper. All authors critically revised the manuscript.

ACKNOWLEDGMENTS

We thank J.-P. Pillot for the pea plant bioassays, Bruno Baron (Institut Pasteur, France) for access to and help with the nanoDSF experiments, Thomas Larribeau for technical assistance, and Catherine Rameau, Sandrine Bonhomme, and Martine De Cock for their comments on the manuscript. The authors declare no conflict of interest.

Received: July 28, 2020
Revised: January 25, 2021
Accepted: January 31, 2021
Published: February 5, 2021

REFERENCES

Arite, T., Umehara, M., Ishikawa, S., Hanada, A., Maekawa, M., Yamaguchi, S., and Kyozuka, J. (2009). *d14*, a strigolactone-insensitive mutant of rice, shows an accelerated outgrowth of tillers. Plant Cell Physiol. **50**:1416–1424.

Auger, B., Pouvreau, J.-B., Pouponneau, K., Yoneyama, K., Montiel, G., Le Bizec, B., Yoneyama, K., Delavault, P., Delourme, R., and Simier, P. (2012). Germination stimulants of *Phelipanche ramosa* in the rhizosphere of *Brassica napus* are derived from the glucosinolate pathway. Mol. Plant Microbe Interact. **25**:993–1004.

Besserer, A., Bécard, G., Jauneau, A., Roux, C., and Sejalon-Delmas, N. (2008). GR24, a synthetic analog of strigolactones, stimulates the

mitosis and growth of the arbuscular mycorrhizal fungus *Gigaspora rosea* by boosting its energy metabolism. Plant Physiol. **148**:402–413.

Boyer, F.-D., de Saint Germain, A., Pillot, J.-P., Pouvreau, J.-B., Chen, V.X., Ramos, S., Stévenin, A., Simier, P., Delavault, P., Beau, J.-M., et al. (2012). Structure-activity relationship studies of strigolactone-related molecules for branching inhibition in garden pea: molecule design for shoot branching. Plant Physiol. **159**:1524–1544.

Boyer, F.-D., de Saint Germain, A., Pouvreau, J.-B., Clavé, G., Pillot, J.-P., Roux, A., Rasmussen, A., Depuydt, S., Lauressergues, D., Frei dit Frey, N., et al. (2014). New strigolactone analogs as plant hormones with low activities in the rhizosphere. Mol. Plant **7**:675–690.

Brun, G., Braem, L., Thoiron, S., Gevaert, K., Goormachtig, S., and Delavault, P. (2017). Seed germination in parasitic plants: what insights can we expect from strigolactone research? J. Exp. Bot. **69**:2265–2280.

Brun, G., Thoiron, S., Braem, L., Pouvreau, J.-B., Montiel, G., Lechat, M.-M., Simier, P., Gevaert, K., Goormachtig, S., and Delavault, P. (2019). CYP707As are effectors of karrikin and strigolactone signalling pathways in *Arabidopsis thaliana* and parasitic plants. Plant Cell Environ. **42**:2612–2626.

Brundrett, M.C., and Tedersoo, L. (2018). Evolutionary history of mycorrhizal symbioses and global host plant diversity. New Phytol. **220**:1108–1115.

Bythell-Douglas, R., Rothfels, C.J., Stevenson, D.W.D., Graham, S.W., Wong, G.K., Nelson, D.C., and Bennett, T. (2017). Evolution of strigolactone receptors by gradual neo-functionalization of KAI2 paralogues. BMC Biol. **15**:52.

Carbonnel, S., Torabi, S., Griesmann, M., Bleek, E., Tang, Y., Buchka, S., Basso, V., Shindo, M., Wang, T.L., Udvardi, M., et al. (2019). Duplicated KAI2 receptors with divergent ligand-binding specificities control distinct developmental traits in *Lotus japonicus*. bioRxiv https://doi.org/10.1101/754937.

Carter, P., and Wells, J.A. (1988). Dissecting the catalytic triad of a serine protease. Nature **332**:564–568.

Conn, C.E., Bythell-Douglas, R., Neumann, D., Yoshida, S., Whittington, B., Westwood, J.H., Shirasu, K., Bond, C.S., Dyer, K.A., and Nelson, D.C. (2015). Convergent evolution of strigolactone perception enabled host detection in parasitic plants. Science **349**:540–543.

Conn, C.E., and Nelson, D.C. (2016). Evidence that KARRIKIN-INSENSITIVE2 (KAI2) receptors may perceive an unknown signal that is not karrikin or strigolactone. Front. Plant Sci. **6**:1219.

de Saint Germain, A., Clavé, G., Badet-Denisot, M.-A., Pillot, J.-P., Cornu, D., Le Caer, J.-P., Burger, M., Pelissier, F., Retailleau, P., Turnbull, C., et al. (2016). An histidine covalent receptor and butenolide complex mediates strigolactone perception. Nat. Chem. Biol. **12**:787–794.

Dekkers, B.J.W., Willems, L., Bassel, G.W., van Bolderen-Veldkamp, R.P., Ligterink, W., Hilhorst, H.W.M., and Bentsink, L. (2011). Identification of reference genes for RT–qPCR expression analysis in *Arabidopsis* and tomato seeds. Plant Cell Physiol. **53**:28–37.

Delavault, P., Montiel, G., Brun, G., Pouvreau, J.B., Thoiron, S., and Simier, P. (2017). Communication between host plants and parasitic plants. Adv. Bot. Res. **82**:55–82.

Fernandez-Aparicio, M., Reboud, X., and Gibot-Leclerc, S. (2016). Broomrape weeds. Underground mechanisms of parasitism and associated strategies for their control: a Review. Front. Plant Sci. **7**:135.

Fernández-Aparicio, M., Rubiales, D., Bandaranayake, P.C.G., Yoder, J.I., and Westwood, J.H. (2011). Transformation and regeneration of the holoparasitic plant *Phelipanche aegyptiaca*. Plant Methods **7**:36.

Fox, J. (2016). Using the R Commander: A Point-And-Click Interface for R (New York: Chapman & Hall/CRC Press).

Goyet, V., Billard, E., Pouvreau, J.-B., Lechat, M.-M., Pelletier, S., Bahut, M., Monteau, F., Spíchal, L., Delavault, P., Montiel, G., et al. (2017). Haustorium initiation in the obligate parasitic plant *Phelipanche ramosa* involves a host-exudated cytokinin signal. J. Exp. Bot. **68**:5539–5552.

Grenz, J.H., and Sauerborn, J. (2007). Mechanisms limiting the geographical range of the parasitic weed *Orobanche crenata*. Agric. Ecosyst. Environ. **122**:275–281.

Guo, Y., Zheng, Z., La Clair, J.J., Chory, J., and Noel, J.P. (2013). Smoke-derived karrikin perception by the alpha/beta-hydrolase KAI2 from *Arabidopsis*. Proc. Natl. Acad. Sci. U S A **110**:8284–8289.

Hamiaux, C., Drummond, R.S.M., Janssen, B.J., Ledger, S.E., Cooney, J.M., Newcomb, R.D., and Snowden, K.C. (2012). DAD2 is an alpha/beta hydrolase likely to be involved in the perception of the plant branching hormone, strigolactone. Curr. Biol. **22**:2032–2036.

Jamil, M., Kountche, B.A., Haider, I., Wang, J.Y., Aldossary, F., Zarban, R.A., Jia, K.P., Yonli, D., Shahul Hameed, U.F., Takahashi, I., et al. (2019). Methylation at the C-3' in D-ring of strigolactone analogs reduces biological activity in root parasitic plants and rice. Front. Plant Sci. **10**:353.

Johnson, A.W., Gowda, G., Hassanali, A., Knox, J., Monaco, S., Razavi, Z., and Rosebery, G. (1981). The preparation of synthetic analogs of strigol. J. Chem. Soc. Perkin Trans. **1**:1734–1743.

Johnson, A.W., Rosebery, G., and Parker, C. (1976). A novel approach to *Striga* and *Orobanche* control using synthetic germination stimulants. Weed Res. **16**:223–227.

Katoh, K., Kuma, K., Toh, H., and Miyata, T. (2005). MAFFT version 5: improvement in accuracy of multiple sequence alignment. Nucleic Acids Res. **33**:511–518.

Katoh, K., Rozewicki, J., and Yamada, K.D. (2019). MAFFT online service: multiple sequence alignment, interactive sequence choice and visualization. Brief. Bioinf. **20**:1160–1166.

Kumar, S., Stecher, G., and Tamura, K. (2016). MEGA7: molecular evolutionary genetics analysis version 7.0 for bigger datasets. Mol. Biol. Evol. **33**:1870–1874.

Lechat, M.-M., Pouvreau, J.-B., Péron, T., Gauthier, M., Montiel, G., Véronési, C., Todoroki, Y., Le Bizec, B., Monteau, F., Macherel, D., et al. (2012). PrCYP707A1, an ABA catabolic gene, is a key component of Phelipanche ramosa seed germination in response to the strigolactone analogue GR24. J. Exp. Bot. **63**:5311–5322. https://doi.org/10.1093/jxb/ers189.

Lechat, M.-M., Brun, G., Montiel, G., Veronesi, C., Simier, P., Thoiron, S., Pouvreau, J.-B., and Delavault, P. (2015). Seed response to strigolactone is controlled by abscisic acid-independent DNA methylation in the obligate root parasitic plant, *Phelipanche ramosa* L. Pomel. J. Exp. Bot. **66**:3129–3140.

Lee, H.W., Sharma, P., Janssen, B.J., Drummond, R.S.M., Luo, Z., Hamiaux, C., Collier, T., Allison, J.R., Newcomb, R.D., and Snowden, K.C. (2020). Flexibility of the petunia strigolactone receptor DAD2 promotes its interaction with signaling partners. J. Biol. Chem. **295**:4181–4193.

Livak, K.J., and Schmittgen, T.D. (2001). Analysis of relative gene expression data using real-time quantitative PCR and the 2(T)(-Delta Delta C) method. Methods **25**:402–408.

Lopez-Obando, M., Ligerot, Y., Bonhomme, S., Boyer, F.-D., and Rameau, C. (2015). Strigolactone biosynthesis and signaling in plant development. Development **142**:3615–3619.

Nakamura, H., Xue, Y.L., Miyakawa, T., Hou, F., Qin, H.M., Fukui, K., Shi, X., Ito, E., Ito, S., Park, S.H., et al. (2013). Molecular mechanism of strigolactone perception by DWARF14. Nat. Commun. **4**:2613.

Parker, C. (2012). Parasitic weeds: a world challenge. Weed Sci. **60**:269–276.

Pepperman, A.B., Connick, W.J., Vail, S.L., Worsham, A.D., Pavlista, A.D., and Moreland, D.E. (1982). Evaluation of precursors and analogs of strigol as witchweed (*Striga asiatica*) seed germination stimulants. Weed Sci. **30**:561–566.

Pickett, J.A., Wadhams, L.J., and Woodcock, C.M. (1997). Developing sustainable pest control from chemical ecology. Agric. Ecosyst. Environ. **64**:149–156.

Pouvreau, J.-B., Gaudin, Z., Auger, B., Lechat, M.M., Gauthier, M., Delavault, P., and Simier, P. (2013). A high-throughput seed germination assay for root parasitic plants. Plant Methods **9**:32.

Rasmussen, A., Mason, M.G., De Cuyper, C., Brewer, P.B., Herold, S., Agusti, J., Geelen, D., Greb, T., Goormachtig, S., Beeckman, T., et al. (2012). Strigolactones suppress adventitious rooting in *Arabidopsis* and pea. Plant Physiol. **158**:1976–1987.

Satchell, D.P.N., Satchell, R.S., and Wassef, W.N. (1990). The kinetics and mechanism of addition of water and alcohols to *p*-nitrophenyl isothiocyanate. The effects of added dimethyl sulfoxide. Z. Naturforsch., B: Chem. Sci. **45**:1032–1036.

Seto, Y., Yasui, R., Kameoka, H., Tamiru, M., Cao, M., Terauchi, R., Sakurada, A., Hirano, R., Kisugi, T., Hanada, A., et al. (2019). Strigolactone perception and deactivation by a hydrolase receptor DWARF14. Nat. Commun. **10**:191.

Shabek, N., Ticchiarelli, F., Mao, H., Hinds, T.R., Leyser, O., and Zheng, N. (2018). Structural plasticity of D3–D14 ubiquitin ligase in strigolactone signalling. Nature **563**:652–656.

Stamatakis, A. (2014). RAxML version 8: a tool for phylogenetic analysis and post-analysis of large phylogenies. Bioinformatics **30**:1312–1313.

Stojanova, B., Delourme, R., Duffé, P., Delavault, P., and Simier, P. (2019). Genetic differentiation and host preference reveal non-exclusive host races in the generalist parasitic weed *Phelipanche ramosa*. Weed Res. **59**:107–118.

Sun, Y.K., Flematti, G.R., Smith, S.M., and Waters, M.T. (2016). Reporter gene-facilitated detection of compounds in *Arabidopsis* leaf extracts that activate the karrikin signaling pathway. Front. Plant Sci. **7**:1799.

Swarbreck, S.M., Guerringue, Y., Matthus, E., Jamieson, F.J.C., and Davies, J.M. (2019). Impairment in karrikin but not strigolactone sensing enhances root skewing in *Arabidopsis thaliana*. Plant J. **98**:607–621.

Takahashi, I., and Asami, T. (2018). Target-based selectivity of strigolactone agonists and antagonists in plants and their potential use in agriculture. J. Exp. Bot. **69**:2241–2254.

Tian, W., Chen, C., Lei, X., Zhao, J., and Liang, J. (2018). CASTp 3.0: computed atlas of surface topography of proteins. Nucleic Acids Res. **46**:W363–W367.

Toh, S., Holbrook-Smith, D., Stogios, P.J., Onopriyenko, O., Lumba, S., Tsuchiya, Y., Savchenko, A., and McCourt, P. (2015). Structure-function analysis identifies highly sensitive strigolactone receptors in *Striga*. Science **350**:203–207.

Toh, S., Kamiya, Y., Kawakami, N., Nambara, E., McCourt, P., and Tsuchiya, Y. (2012). Thermoinhibition uncovers a role for strigolactones in *Arabidopsis* seed germination. Plant Cell Physiol **53**:107–117.

Tsuchiya, Y., Yoshimura, M., Sato, Y., Kuwata, K., Toh, S., Holbrook-Smith, D., Zhang, H., McCourt, P., Itami, K., Kinoshita, T., et al. (2015). Probing strigolactone receptors in *Striga hermonthica* with fluorescence. Science **349**:864–868.

Uraguchi, D., Kuwata, K., Hijikata, Y., Yamaguchi, R., Imaizumi, H., Am, S., Rakers, C., Mori, N., Akiyama, K., Irle, S., et al. (2018). A femtomolar-range suicide germination stimulant for the parasitic plant *Striga hermonthica*. Science **362**:1301.

Villaécija-Aguilar, J.A., Hamon-Josse, M., Carbonnel, S., Kretschmar, A., Schmidt, C., Dawid, C., Bennett, T., and Gutjahr, C. (2019). SMAX1/SMXL2 regulate root and root hair development downstream of KAI2-mediated signalling in *Arabidopsis*. PLOS Genet. **15**:e1008327.

Vurro, M., Prandi, C., and Baroccio, F. (2016). Strigolactones: how far is their commercial use for agricultural purposes? Pest Manage. Sci. **72**:2026–2034.

Waterhouse, A., Bertoni, M., Bienert, S., Studer, G., Tauriello, G., Gumienny, R., Heer, F.T., de Beer, T.A.P., Rempfer, C., Bordoli, L., et al. (2018). SWISS-MODEL: homology modelling of protein structures and complexes. Nucleic Acids Res. **46**:W296–W303.

Waters, M.T. (2019). Spoilt for choice: new options for inhibitors of strigolactone signaling. Mol. Plant **12**:21–23.

Waters, M.T., Gutjahr, C., Bennett, T., and Nelson, D.C. (2017). Strigolactone signaling and evolution. Annu. Rev. Plant Biol. **68**:291–322.

Waters, M.T., Nelson, D.C., Scaffidi, A., Flematti, G.R., Sun, Y.K., Dixon, K.W., and Smith, S.M. (2012). Specialisation within the DWARF14 protein family confers distinct responses to karrikins and strigolactones in *Arabidopsis*. Development **139**:1285–1295.

Wicke, S., Müller, K.F., dePamphilis, C.W., Quandt, D., Bellot, S., and Schneeweiss, G.M. (2016). Mechanistic model of evolutionary rate variation en route to a nonphotosynthetic lifestyle in plants. Proc. Natl. Acad. Sci. U.S.A. **113**:9045.

Xu, Y., Miyakawa, T., Nosaki, S., Nakamura, A., Lyu, Y., Nakamura, H., Ohto, U., Ishida, H., Shimizu, T., Asami, T., et al. (2018). Structural analysis of HTL and D14 proteins reveals the basis for ligand selectivity in *Striga*. Nat. Commun. **9**:3947.

Yamauchi, M., Ueno, K., Furumoto, T., Wakabayashi, T., Mizutani, M., Takikawa, H., and Sugimoto, Y. (2018). Stereospecific reduction of the butenolide in strigolactones in plants. Bioorg. Med. Chem. **26**:4225–4233.

Yang, Z., Zhang, Y., Wafula, E.K., Honaas, L.A., Ralph, P.E., Jones, S., Clarke, C.R., Liu, S., Su, C., Zhang, H., et al. (2016). Horizontal gene transfer is more frequent with increased heterotrophy and contributes to parasite adaptation. Proc. Natl. Acad. Sci. U.S.A. **113**:E7010.

Yao, J., Mashiguchi, K., Scaffidi, A., Akatsu, T., Melville, K.T., Morita, R., Morimoto, Y., Smith, S.M., Seto, Y., Flematti, G.R., et al. (2018a). An allelic series at the KARRIKIN INSENSITIVE 2 locus of *Arabidopsis thaliana* decouples ligand hydrolysis and receptor degradation from downstream signalling. Plant J. **96**:75–89.

Yao, R., Ming, Z., Yan, L., Li, S., Wang, F., Ma, S., Yu, C., Yang, M., Chen, L., Li, Y., et al. (2016). DWARF14 is a non-canonical hormone receptor for strigolactone. Nature **536**:469–473.

Yao, R., Wang, F., Ming, Z.H., Du, X.X., Chen, L., Wang, Y.P., Zhang, W.H., Deng, H.T., and Xie, D.X. (2017). ShHTL7 is a non-canonical receptor for strigolactones in root parasitic weeds. Cell Res **27**:838–841.

Yao, R., Wang, L., Li, Y., Chen, L., Li, S., Du, X., Wang, B., Yan, J., Li, J., and Xie, D. (2018b). Rice DWARF14 acts as an unconventional hormone receptor for strigolactone. J. Exp. Bot. **69**:2355–2365.

Yoneyama, K. (2016). Small-molecule inhibitors: weed-control measures. Nat. Chem. Biol. **12**:658–659.

Zehhar, N., Ingouff, M., Bouya, D., and Fer, A. (2002). Possible involvement of gibberellins and ethylene in *Orobanche ramosa* germination. Weed Res. **42**:464–469.

Zwanenburg, B., and Pospíšil, T. (2013). Structure and activity of strigolactones: new plant hormones with a rich future. Mol. Plant **6**:38–62.

Plant Communications, Volume *2*

Supplemental information

A *Phelipanche ramosa* KAI2 protein perceives strigolactones and isothiocyanates enzymatically

Alexandre de Saint Germain, Anse Jacobs, Guillaume Brun, Jean-Bernard Pouvreau, Lukas Braem, David Cornu, Guillaume Clavé, Emmanuelle Baudu, Vincent Steinmetz, Vincent Servajean, Susann Wicke, Kris Gevaert, Philippe Simier, Sofie Goormachtig, Philippe Delavault, and François-Didier Boyer

Supplementary Figures and Tables

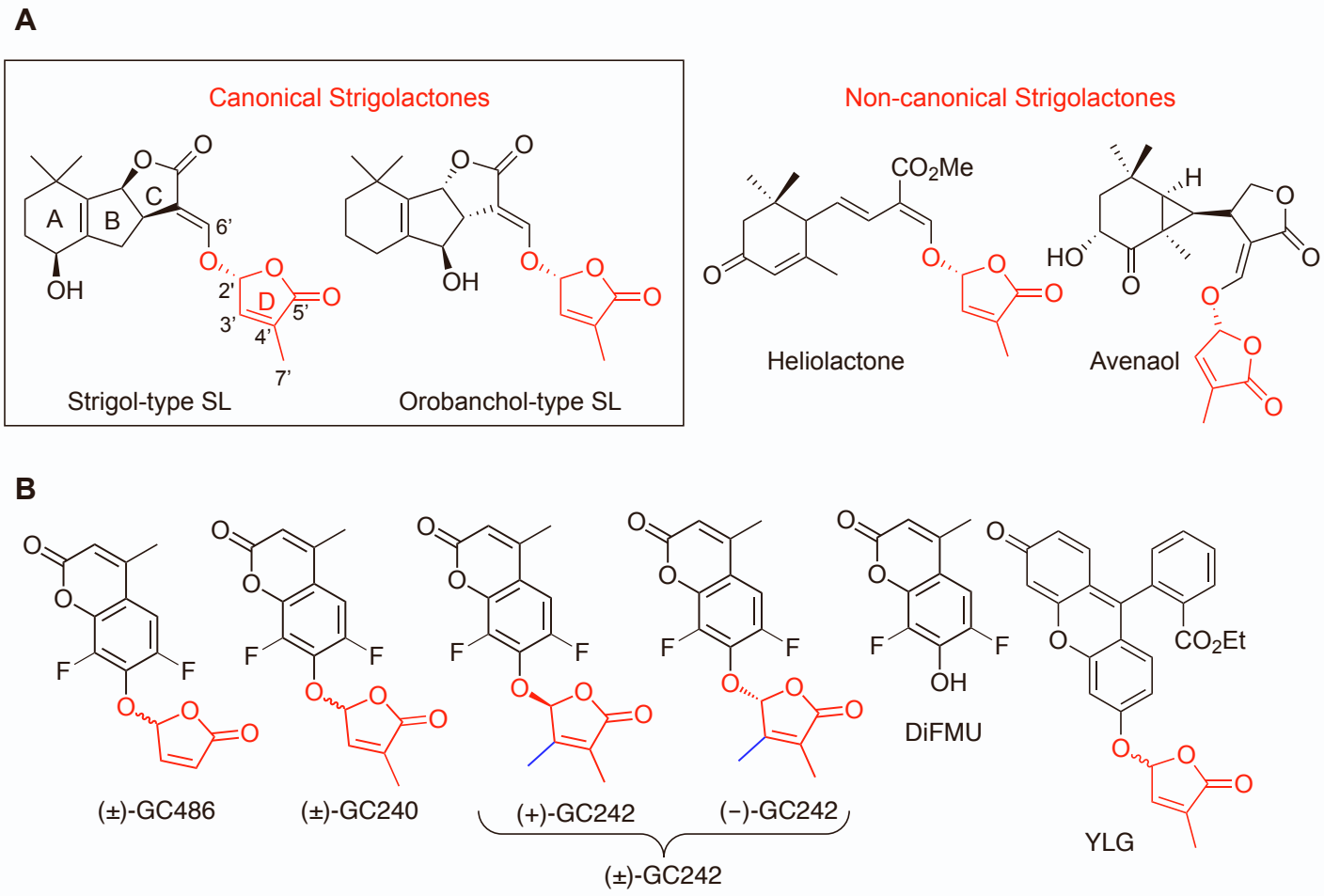

Supplementary Figure 1. Chemical structures. (A) Natural strigolactones. **(B)** Profluorescent probes. GC series and Yoshimulactone (YLG).

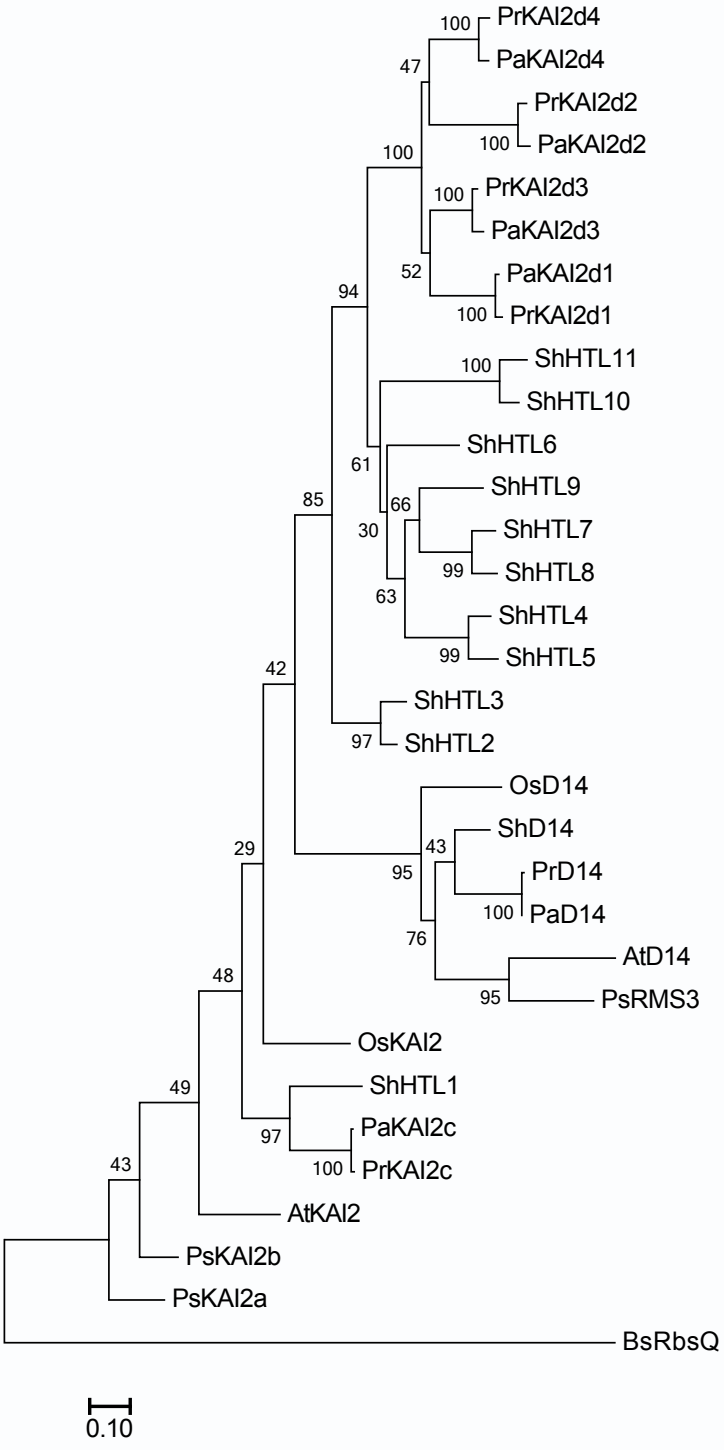

Supplementary Figure 2. Phylogenetic analysis of KAI2 and D14 nucleotide sequences. The phylogenetic tree was constructed with the maximum likelihood method and 1,000 bootstraps replicates by means of RAxML. Scale bar = 0.1 substitutions per site.

Data file S1. D14 and KAI2 amino acid sequences
Data file S2. D14 and KAI2 nucleotide sequences
Data file S3. MAFFT alignement of D14 and KAI2 amino acid sequences
Data file S4. MAFFT alignement of D14 and KAI2 nucleotide sequences
Data file S5. Trimmed MAFFT alignement of D14 and KAI2 amino acid sequences
Data file S6. Trimmed MAFFT alignement of D14 and KAI2 nucleotide sequences

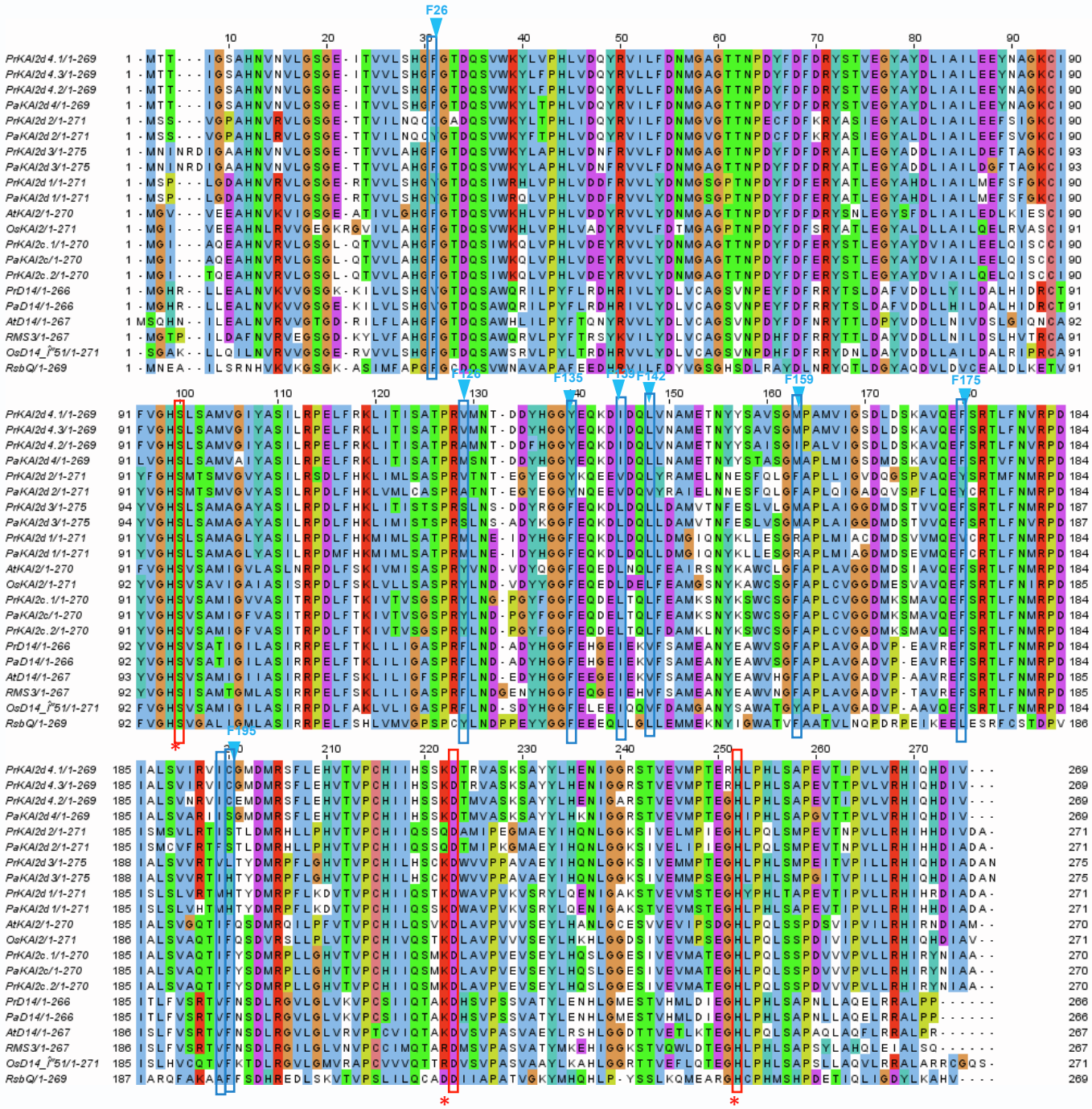

Supplementary Figure 3. Sequence alignment of *Phelipanche ramosa* (*Pr*) and *P. aegyptiaca* (*Pa*) KAI2 protein with D14 and KAI2 proteins from *Arabidopsis* (At), rice (Os), pea (RMS), and the bacterial RbsQ. The three amino acid residues corresponding to the catalytic triad are marked with asterisks. Amino residues highlighted in the Figure 1**B** are indicated with a blue arrowhead. Amino acid numbers are indicated for AtD14. Note that the rice OsD14 protein has a non-conserved 50-amino-acid N-terminal extension omitted in the alignment.

A

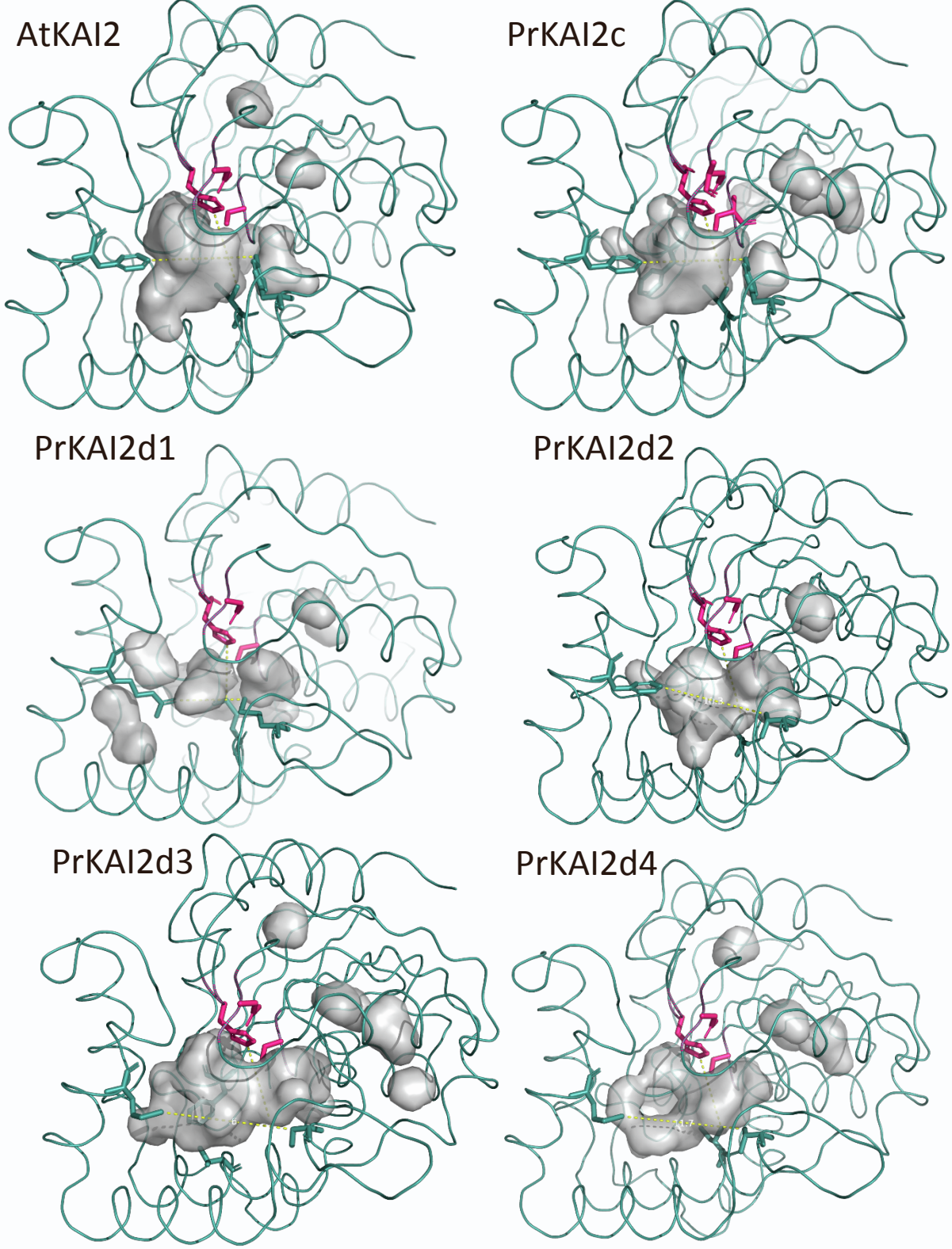

B

Protein	Distance position 124-157 (Å)	Distance position 246-193 (Å)
AtKAI2	10.643	7.693
PrKAI2c	9.996	7.619
PrKAI2d1	6.612	6.168
PrKAI2d2	10.269	7.649
PrKAI2d3	11.598	7.468
PrKAI2d4	11.658	7.637

Supplementary Figure 4. Models of the ligand pockets of the *P. ramosa* KAI2 proteins. (A) Visual representation (different from Figure 1c) of the ligand pockets of the *P. ramosa* KAI2 proteins. The KAI2 protein sequences were modeled with the chain A of the karrikin-bound *Arabidopsis* KAI2 structure as a template (PDB: 4JYP). The protein structures were generated with PYMOL and the cavities within the homology models were visualized with the surface mode on the setting “cavities and pockets culled” within PYMOL. The sticks represent parts of the catalytic triad (Ser, His, Asp). **(B)** Width/length of the ligand pockets of the *P. ramosa* KAI2 proteins.

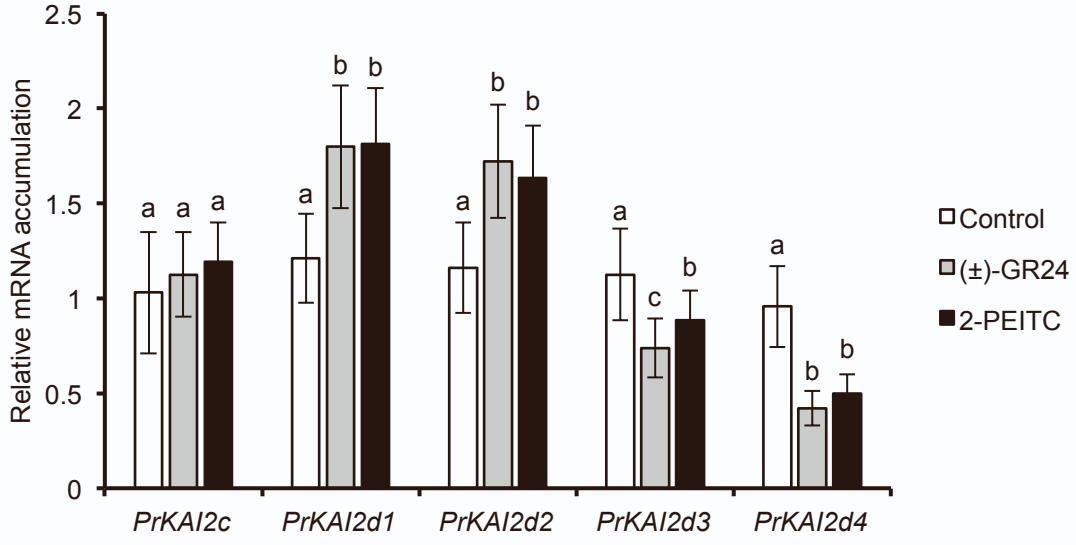

Supplementary Figure 5. Expression of the KAI2 genes in *P. ramosa*. RNA was isolated from seeds conditioned for 7 d, and seeds treated for 6 h with mock (control) or 0.1 µM of the indicated stimulant. *EF1-α* was used as the reference gene, and expression in mock- and stimulant-treated seeds was normalized to gene expression in seeds conditioned for 7 d (ΔΔCt). Data are means ± standard error (n = 3). Letters indicate significant differences in expression between conditions ($P < 0.001$, Tukey-HSD test).

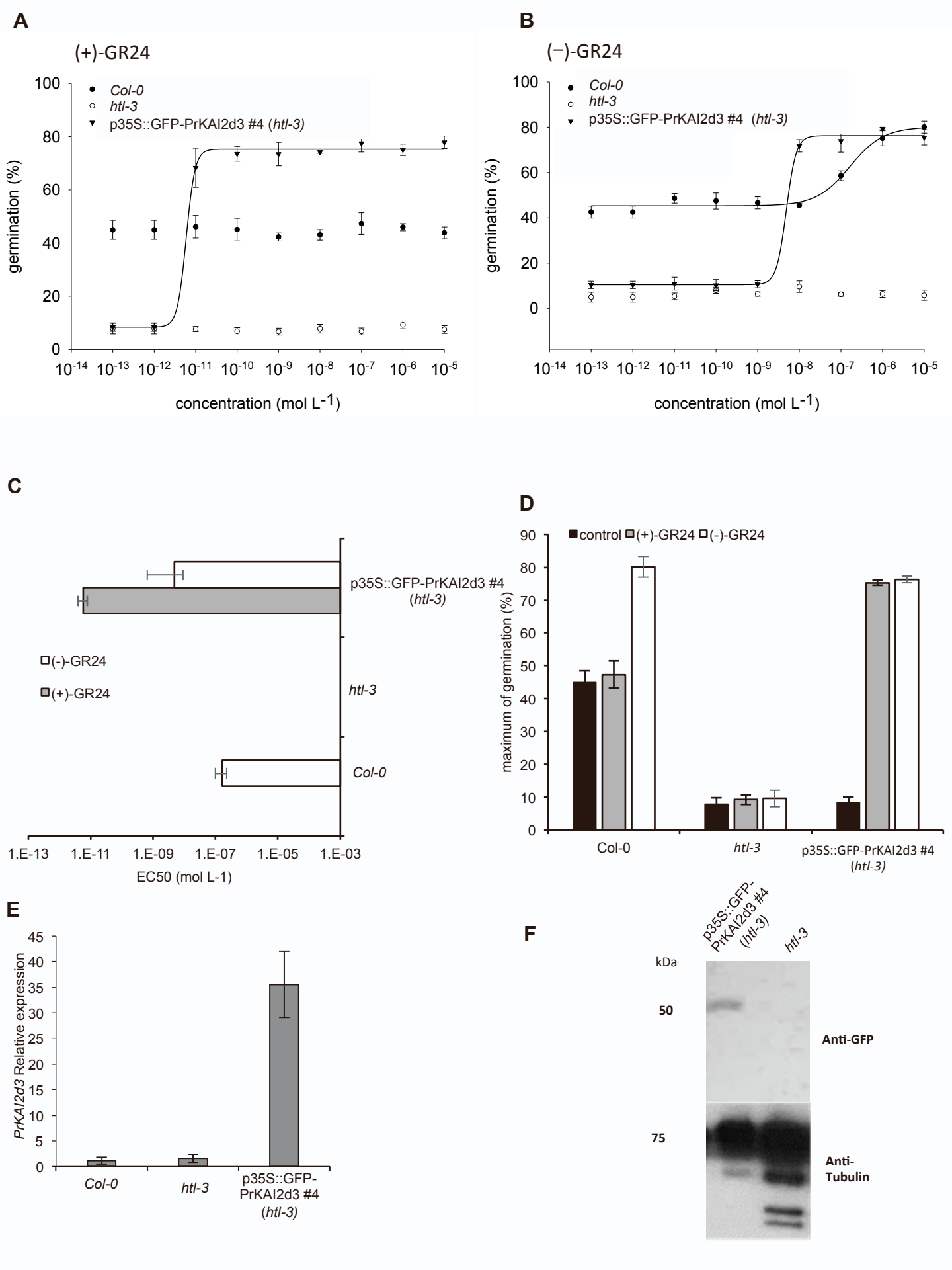
A
(+)-GR24
Col-0
htl-3
p35S::GFP-PrKAI2d3 #4 (htl-3)
germination (%)
concentration (mol L-1)
B
(−)-GR24
Col-0
htl-3
p35S::GFP-PrKAI2d3 #4 (htl-3)
germination (%)
concentration (mol L-1)
C
p35S::GFP-PrKAI2d3 #4 (htl-3)
(-)-GR24
(+)-GR24
htl-3
Col-0
EC50 (mol L-1)
D
control
(+)-GR24
(-)-GR24
maximum of germination (%)
Col-0
htl-3
p35S::GFP-PrKAI2d3 #4 (htl-3)
E
PrKAI2d3 Relative expression
Col-0
htl-3
p35S::GFP-PrKAI2d3 #4 (htl-3)
F
p35S::GFP-PrKAI2d3 #4 (htl-3)
htl-3
kDa
50
75
Anti-GFP
Anti-Tubulin

Supplementary Figure 6. Dose response germination stimulant activities of (+)-GR24 and (−)-GR24 with *Arabidopsis* lines. Dose response germination stimulation activities and modeled curves of (+)-GR24 **(A)** and (−)-GR24 **(B)** on seeds of *Arabidopsis* Col-0 and *htl-3*/p35S::PrKAI2d3. **(C)** Half maximal effective concentration (EC_{50}). **(D)** Maximum germination stimulation activities. Data are indicated ± SE. **(E)** Relative accumulation of *PrKAI2d3* transcripts in *Arabidopsis* Col-0, *htl-3,* and p35S::GFP-PrKAI2d3 #4 (*htl-3*) seeds imbibed for 24 h. **(F)** Accumulation of PrKAI2d3 proteins in *Arabidopsis* p35S::GFP-PrKAI2d3 #4 (*htl-3*) and *htl-3* 5d-old seedlings.

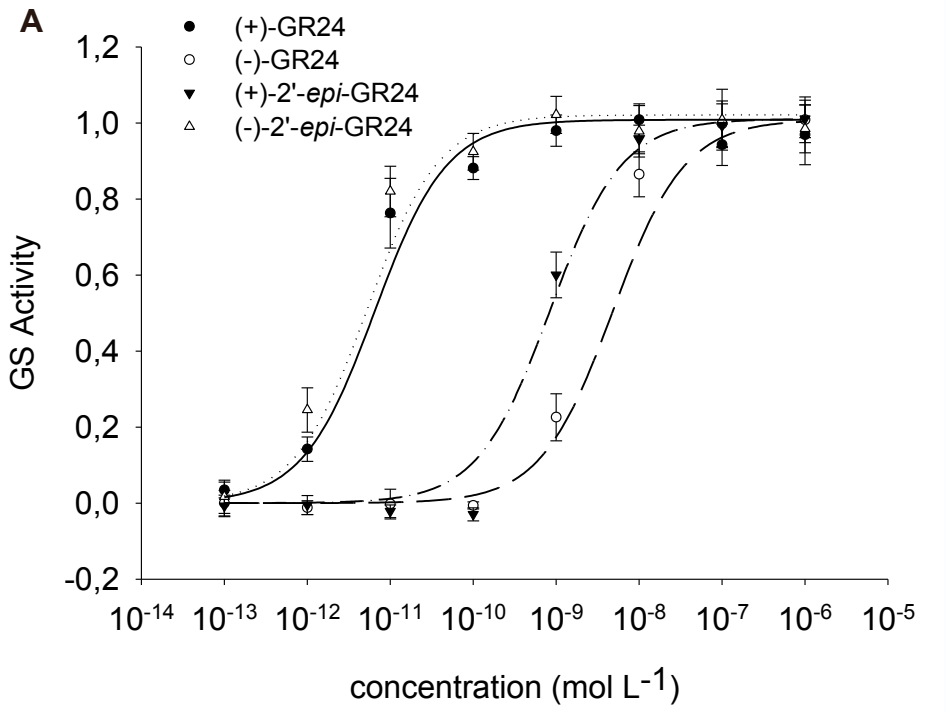

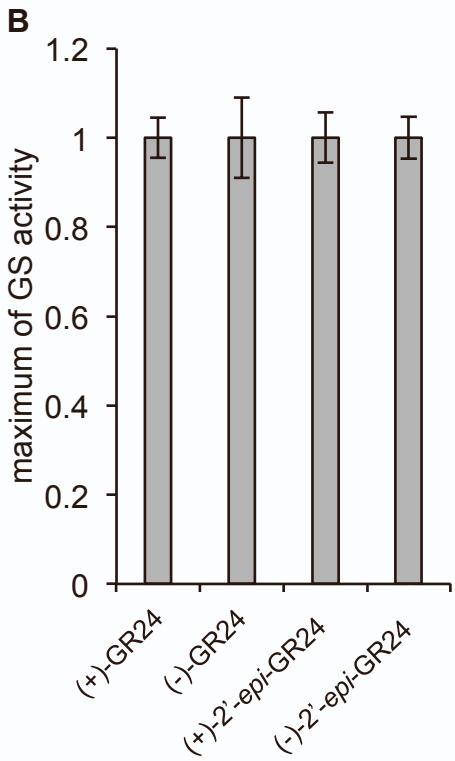

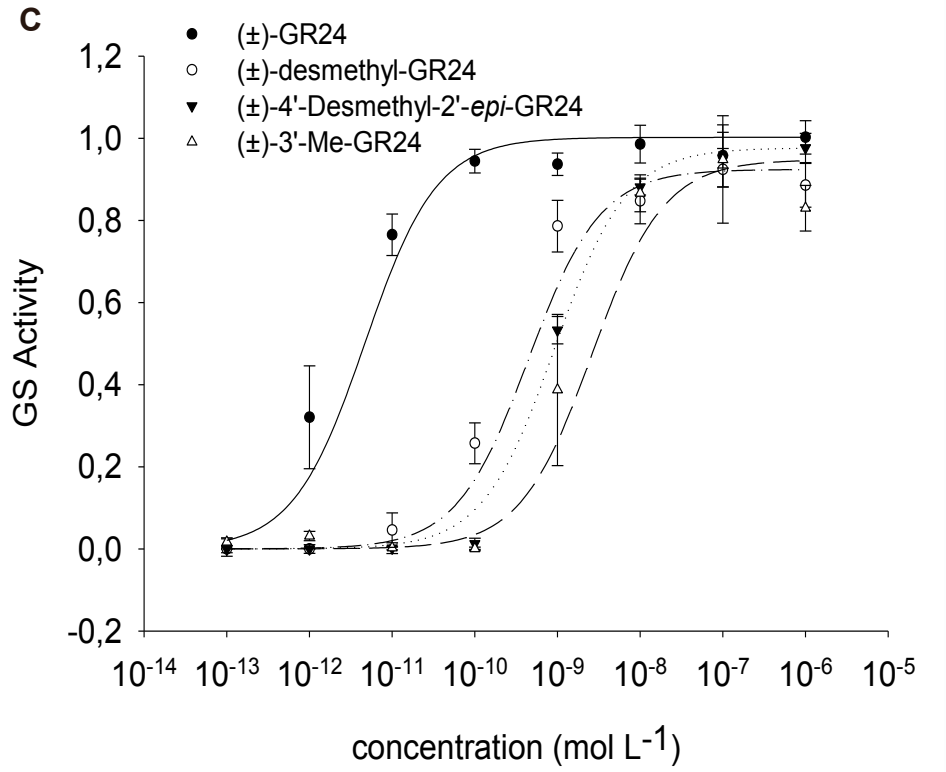

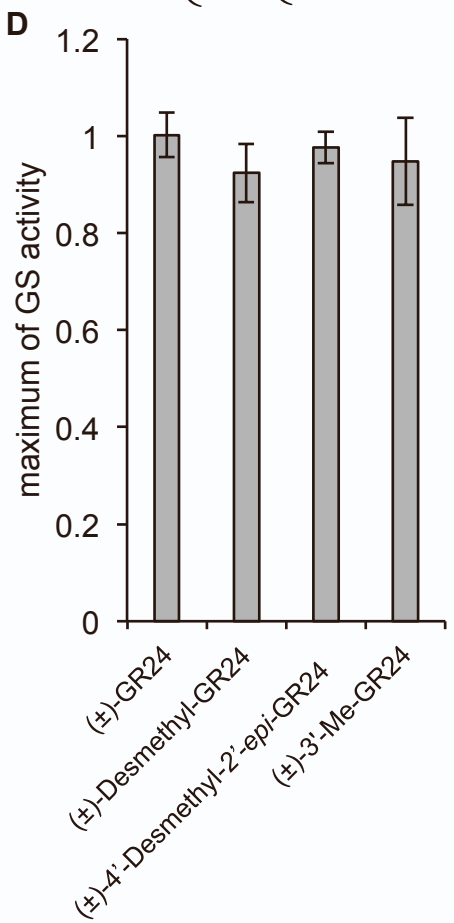

Supplementary Figure 7. Germination assay on *P. ramosa* parasitic-plant seeds of GR24 isomers [(+)-GR24, (−)-GR24, (+)-2'-*epi*-GR24, and (−)-2'-*epi*-GR24] and methyl variation on the GR24 D-ring [(±)-Desmethyl-GR24, (±)-4'-Desmethyl-2'-epi-GR24, and (±)-3'-Me-GR24]. **(A**) and **(C)** Dose response germination stimulation activities and modeled curves.**(B)** and (**D)** Maximum germination stimulation activity relative to (±)-GR24 (1 µM). Data are indicated ± SE.

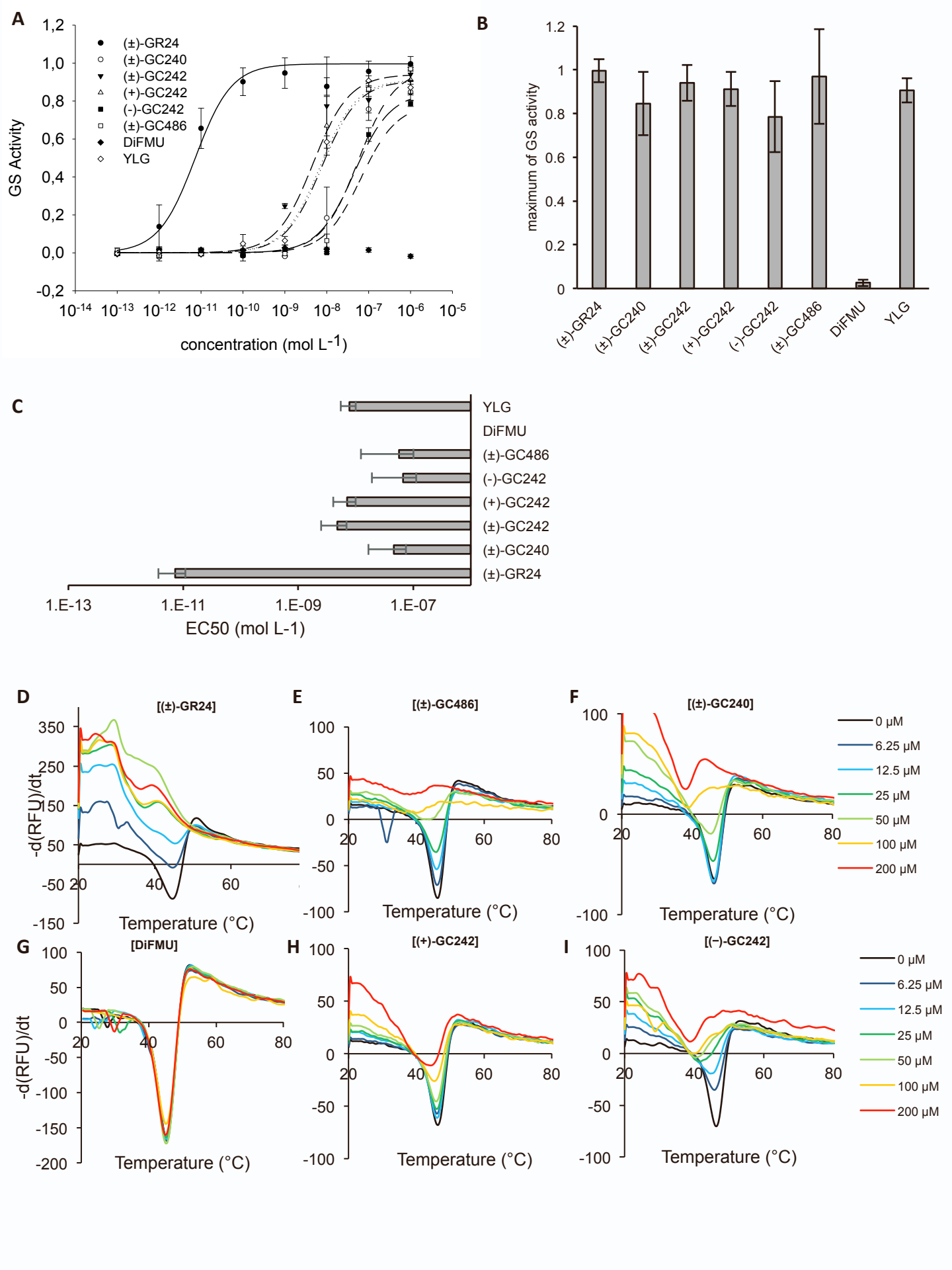
A
GS Activity
concentration (mol L-1)
(±)-GR24
(±)-GC240
(±)-GC242
(+)-GC242
(-)-GC242
(±)-GC486
DiFMU
YLG
B
maximum of GS activity
C
EC50 (mol L-1)
D
[(±)-GR24]
E
[(±)-GC486]
F
[(±)-GC240]
G
[DiFMU]
H
[(+)-GC242]
I
[(−)-GC242]
-d(RFU)/dt
Temperature (°C)
0 µM
6.25 µM
12.5 µM
25 µM
50 µM
100 µM
200 µM

Supplementary Figure 8. Germination assay on *P. ramosa* parasitic-plant seeds of various profluorescent ligands and biochemical analysis of the interaction between PrKAI2d3 and various ligands by DSF. (A) Dose response germination stimulation activities and modeled curves. **(B)** Maximum germination stimulant activity relative to (±)-GR24 (1 µM). **(C)** Half maximal effective concentration (EC_{50}) (mol L^{-1}). Data are indicated ± SE. **(D-I)** Melting temperature curves of PrKAI2d3 with (±)-GR24 **(D)**, (±)-GC486 **(E)**, (±)-GC240 **(F)**, DiFMU **(G)**, (+)-GC242 **(H),** and (−)-GC242 **(I)** at varying concentrations assessed by DSF. Each line represents the average protein melt curve for three technical replicates and the experiment was carried out twice.

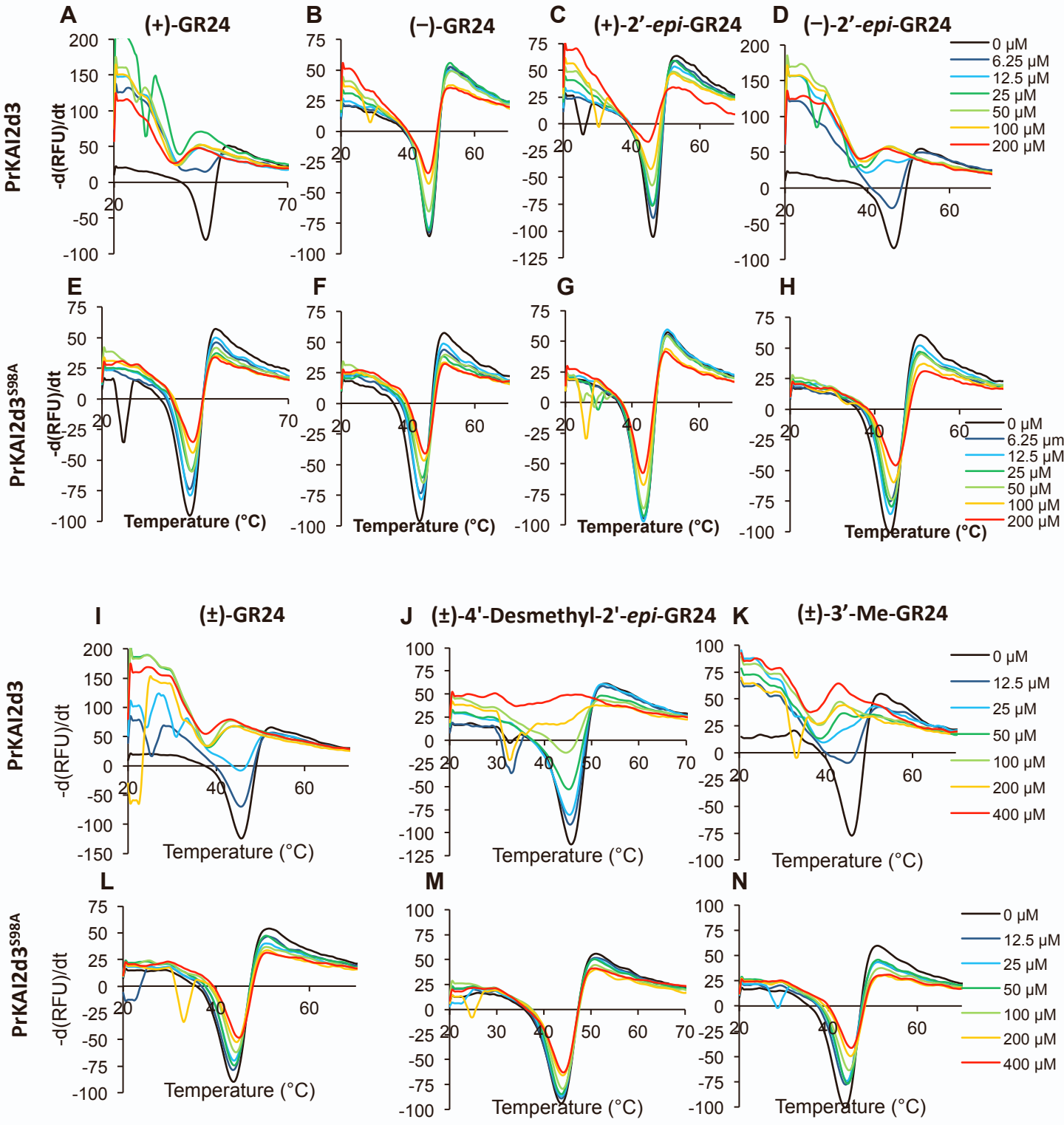

Supplementary Figure 9. Biochemical analysis of the interaction between PrKAI2d3 (A-D, I-K) or PrKAI2d3^{S98A} (E-H, L-N) and various ligands by DSF. Melting temperature curves of PrKAI2d3 or PrKAI2d3^{S98A} at 10 µM with (+)-GR24 **(A, E)**, (−)-GR24 **(B, F)**, (+)-2'-*epi*-GR24 **(C, G)**, (−)-2'-*epi*-GR24 **(D, H)**, (±)-GR24 **(I, L)**, (±)-4'-desmethyl-2'-*epi*-GR24 **(J, M)**, or (±)-3'-Me-GR24 **(K, N)** at varying concentrations assessed by DSF. Each line represents the average protein melt curve for three technical replicates and the experiment was carried out twice.

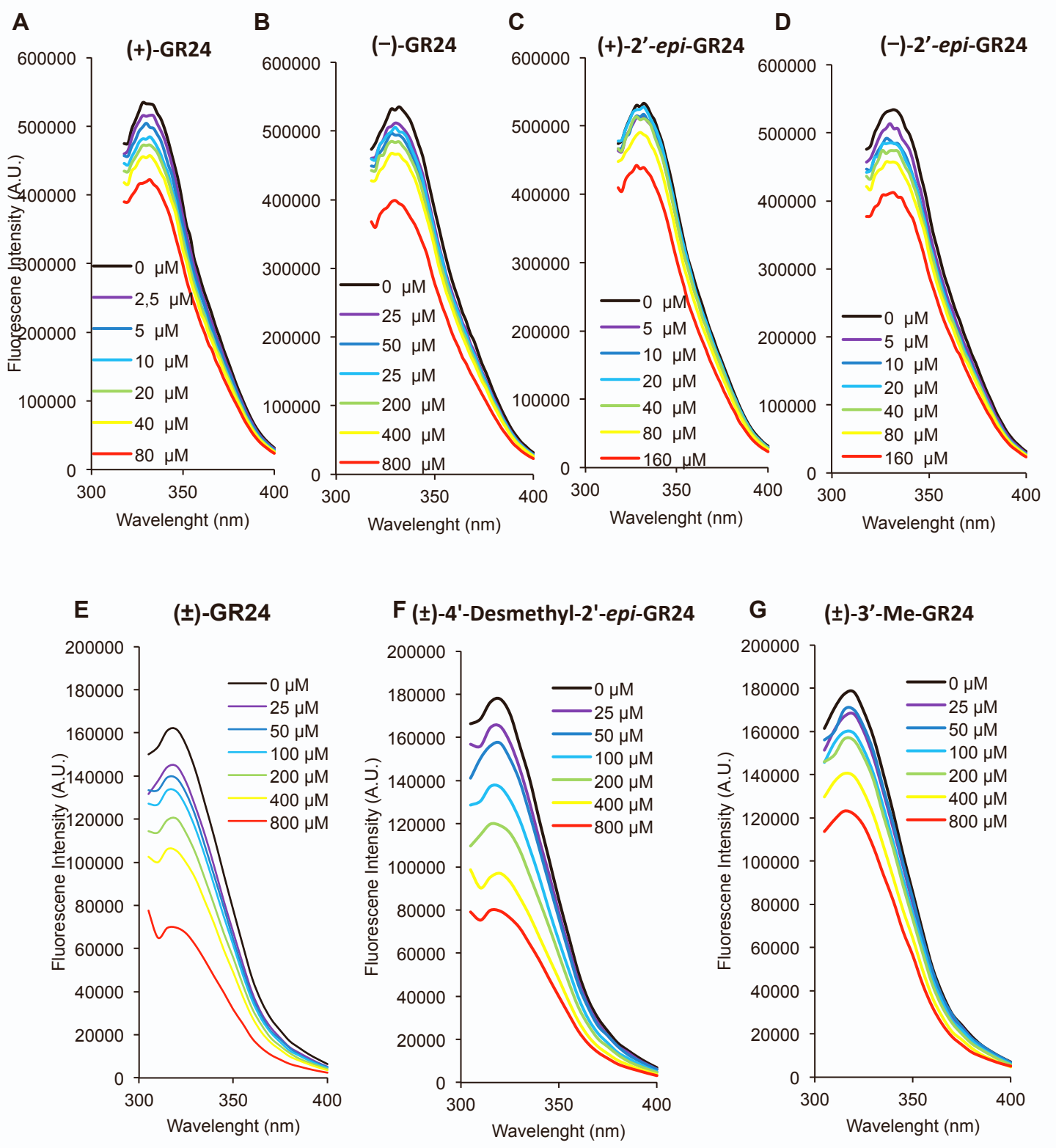

Supplementary Figure 10. Intrinsic tryptophan fluorescence of PrKAI2d3 in the presence of SL analogs. Changes in intrinsic fluorescence emission spectra of PrKAI2d3 in the presence of various concentrations of (+)-GR24 **(A)**, (−)-GR24 **(B)**, (+)-2'-*epi*-GR24 **(C)**, (−)-2'-*epi*-GR24 **(D)**, (±)-GR24 **(E)**, (±)-4'-desmethyl-2'-*epi*-GR24 **(F)**, or (±)-3'-Me-GR24 **(G)**. Proteins (10 µM) were incubated with increasing amounts of ligand (0–800 µM from top to bottom). The observed relative changes in intrinsic fluorescence were plotted as a function of the SL analog concentration, transformed to a saturation degree, and used to determine the apparent K_D values relevant to Figure 2**H,I**. The plots represent the mean of two replicates and the experiments were repeated at least three times. The analysis was done with GraphPad Prism 7.05 Software.

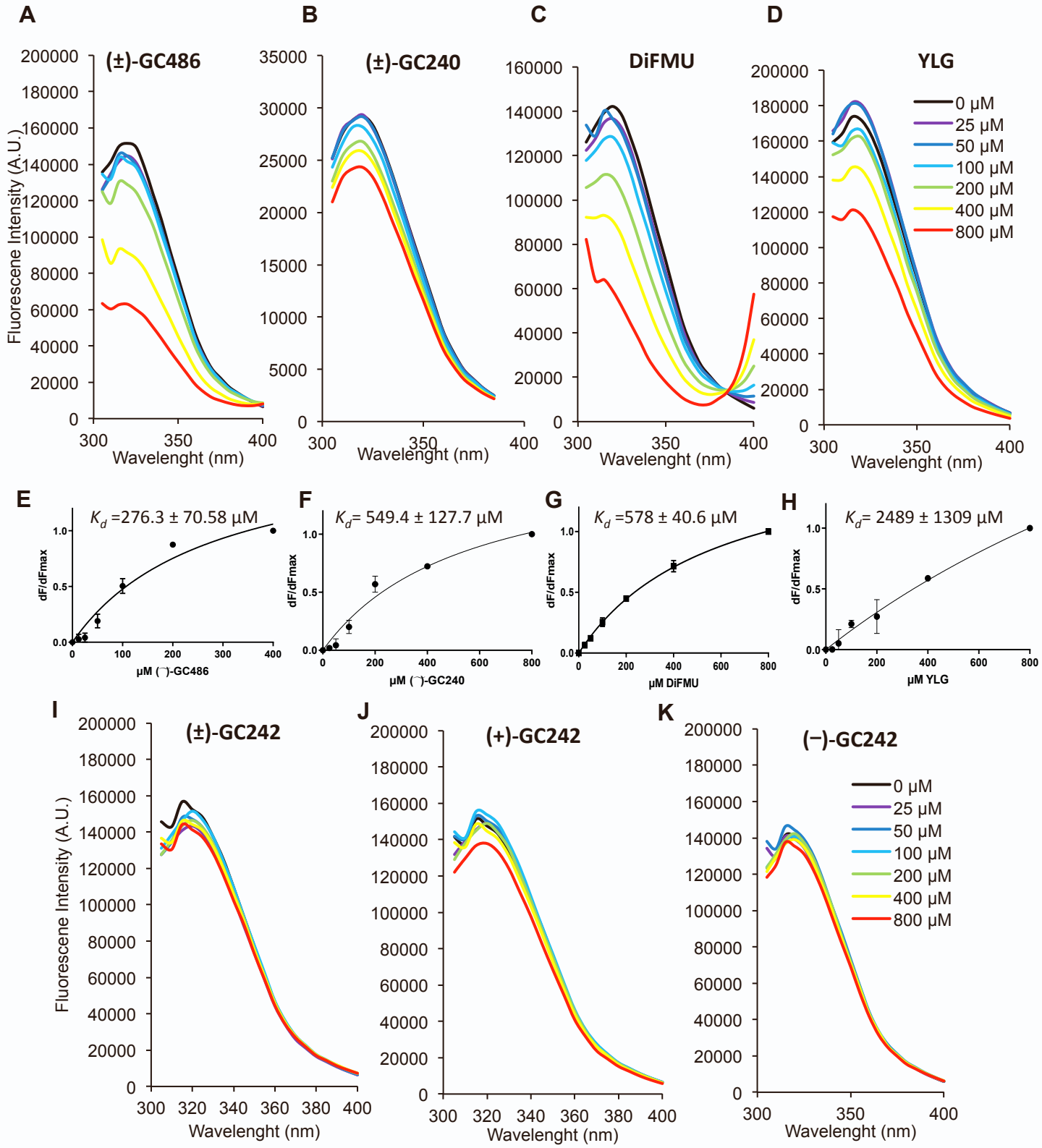
A
(±)-GC486
B
(±)-GC240
C
DiFMU
D
YLG
Fluorescene Intensity (A.U.)
Wavelenght (nm)
0 µM
25 µM
50 µM
100 µM
200 µM
400 µM
800 µM
E
K_d =276.3 ± 70.58 µM
F
K_d= 549.4 ± 127.7 µM
G
K_d =578 ± 40.6 µM
H
K_d= 2489 ± 1309 µM
dF/dFmax
µM (⁻)-GC486
µM (⁻)-GC240
µM DiFMU
µM YLG
I
(±)-GC242
J
(+)-GC242
K
(−)-GC242

Supplementary Figure 11. Intrinsic tryptophan fluorescence of PrKAI2d3 in the presence of profluorescent SL probes. Changes in intrinsic fluorescence emission spectra of PrKAI2d3 in the presence of various concentrations of (±)-GC486 (**A**), (±)-GC240 (**B**), DiFMU (**C**), YLG (**D**), (±)-GC242 (**I**), (+)-GC242 (**J**), or (−)-GC242 (**K**). Proteins (10 µM) were incubated with increasing amounts of ligand (0–800 µM from top to bottom). The observed relative changes in intrinsic fluorescence were plotted as a function of the SL analog concentration and transformed to saturation. Plots of fluorescence intensity *versus* (±)-GC486 (**E**), (±)-GC240 (**F**), DiFMU (**G**), and YLG (**H**) concentrations used to determine the apparent K_D values. The plots represent the mean of two replicates and the experiments were repeated at least three times. The analysis was done with GraphPad Prism 7.05 Software.

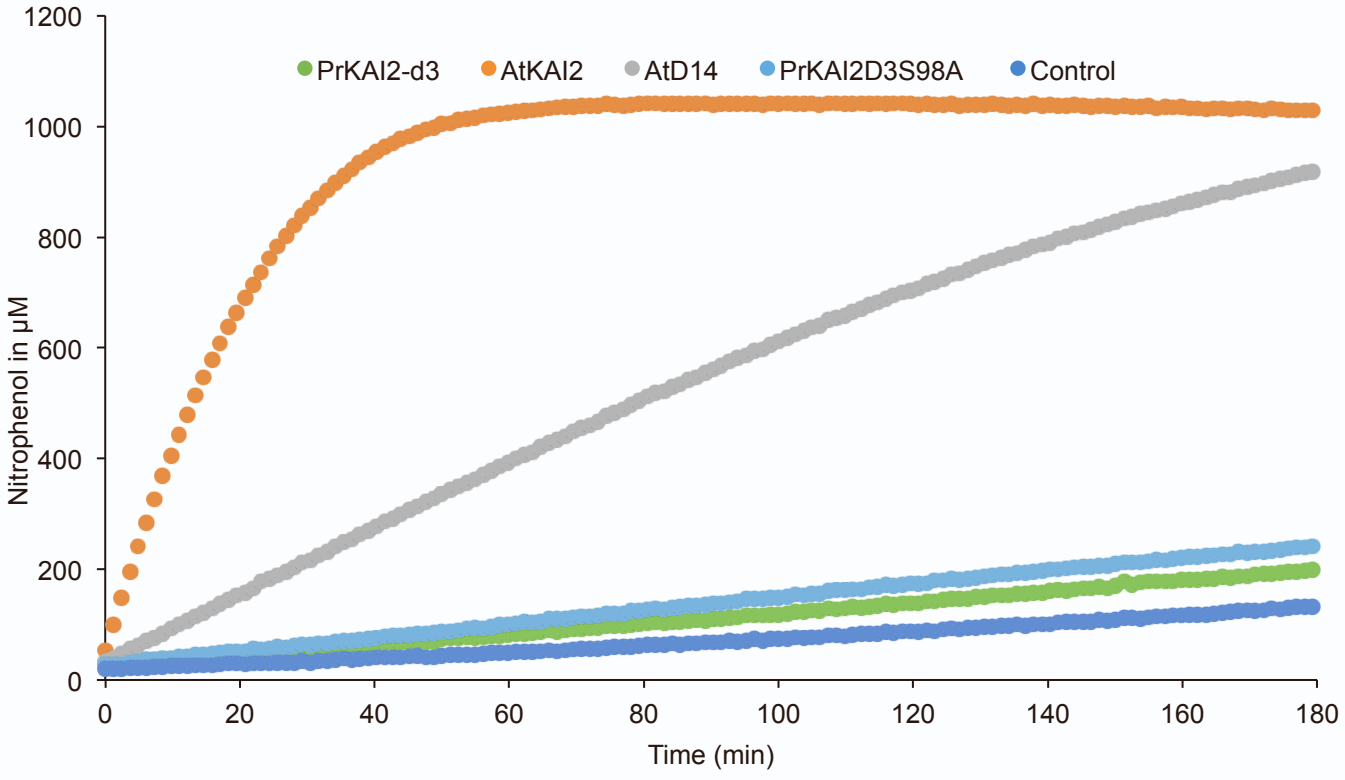

Supplementary Figure 12. PrKAI2d3 hydrolysis activity. Progress curves during the 4-nitrophenyl acetate (*p*-NPA) (1 mM) hydrolysis by PrKAI2d3, PrKAI2d3^{S98A}, AtKAI2, and AtD14 (4 µM). The *p*-NPA release was monitored (A_{405}) at 25 °C.

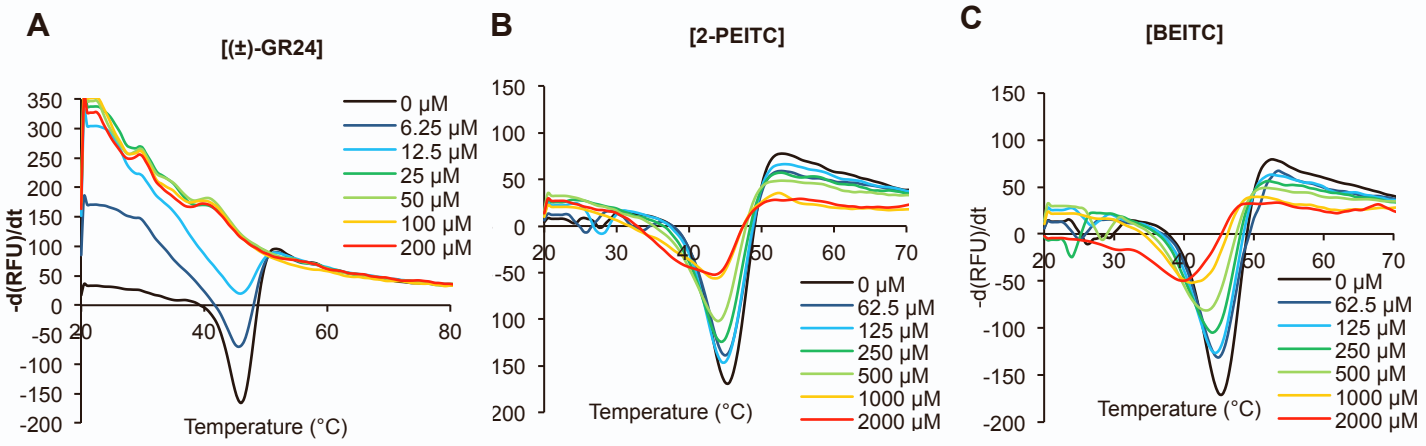

Supplementary Figure 13. Biochemical analysis of the interaction between PrKAI2d3 and ITCs by DSF. Melting temperature curves of PrKAI2d3 at 10 µM with (±)-GR24 **(A)**, 2-PEITC **(B)**, or BITC **(C)** at varying concentrations assessed by DSF. Each line represents the average protein melt curve for three technical replicates and the experiment was carried out twice.

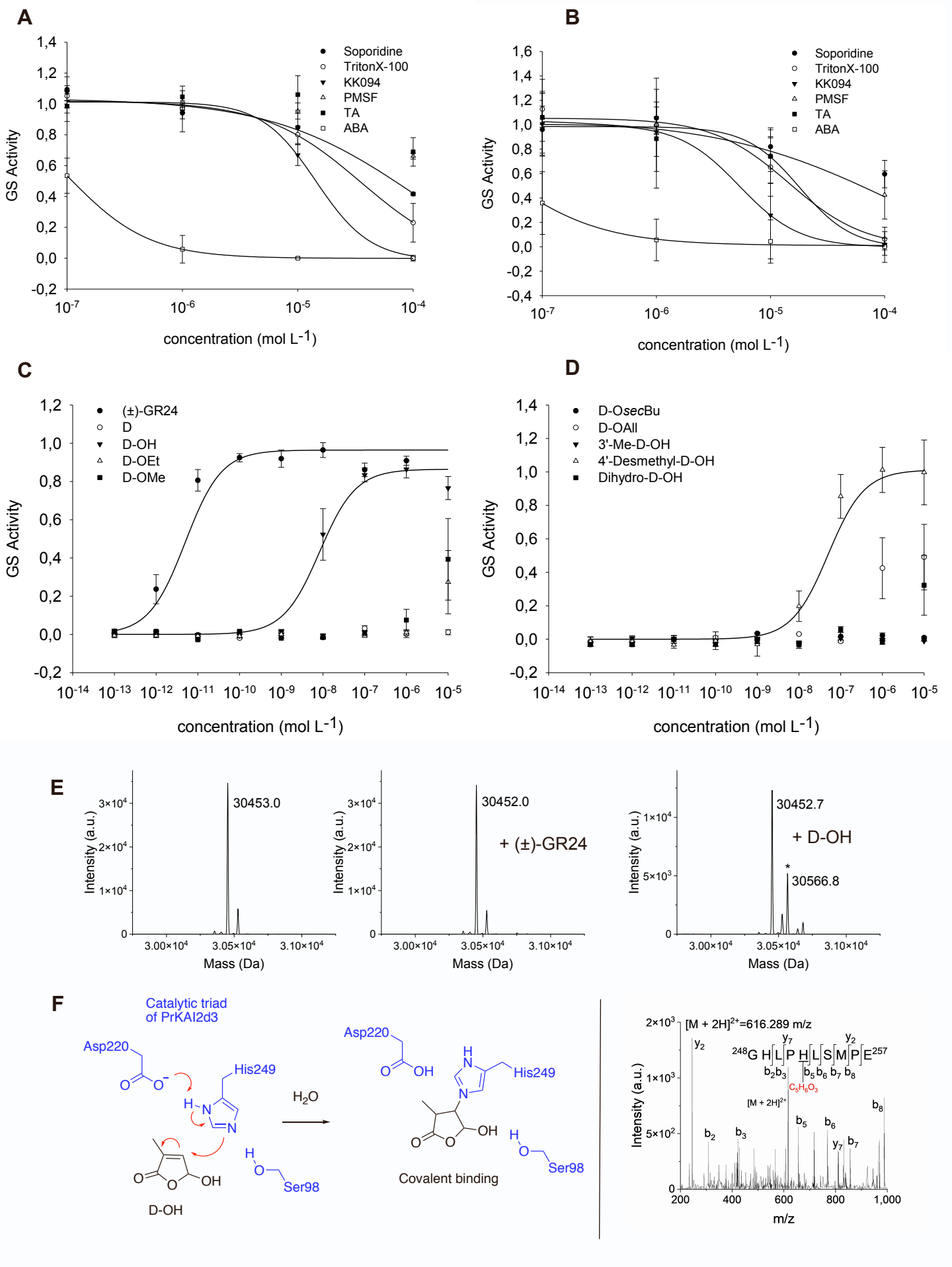
A
B
C
D
E
F
GS Activity
concentration (mol L-1)
Soporidine
TritonX-100
KK094
PMSF
TA
ABA
(±)-GR24
D
D-OH
D-OEt
D-OMe
D-OsecBu
D-OAll
3'-Me-D-OH
4'-Desmethyl-D-OH
Dihydro-D-OH
Intensity (a.u.)
Mass (Da)
30453.0
30452.0
+ (±)-GR24
30452.7
+ D-OH
30566.8
Catalytic triad
of PrKAI2d3
Asp220
His249
Ser98
H2O
D-OH
Covalent binding
[M + 2H]2+=616.289 m/z
m/z

Supplementary Figure 14. Germination inhibition by various chemicals and stimulation by D-analogs. Dose response germination stimulation (GS) activities with 10 nM (±)-GR24 **(A)** and 100 nM 2-PEITC (**B)** and modeled curves **(C**) and (**D)**. Maximum of germination stimulation activity relative to (±)-GR24 (1 µM). Data are indicated ± SE. **(E)** Putative adduct formed after incubation of D-OH with PrKAI2d3. **(F)** Deconvoluted electrospray mass spectra of PrKAI2d3^{S98A} alone, after addition of the D-OH ligand (10 mM) and after addition of the (±)-GR24 ligand (1 mM). The mass increments were measured for the PrKAI2d3^{S98A}-D-OH complex, 114.2 Da.

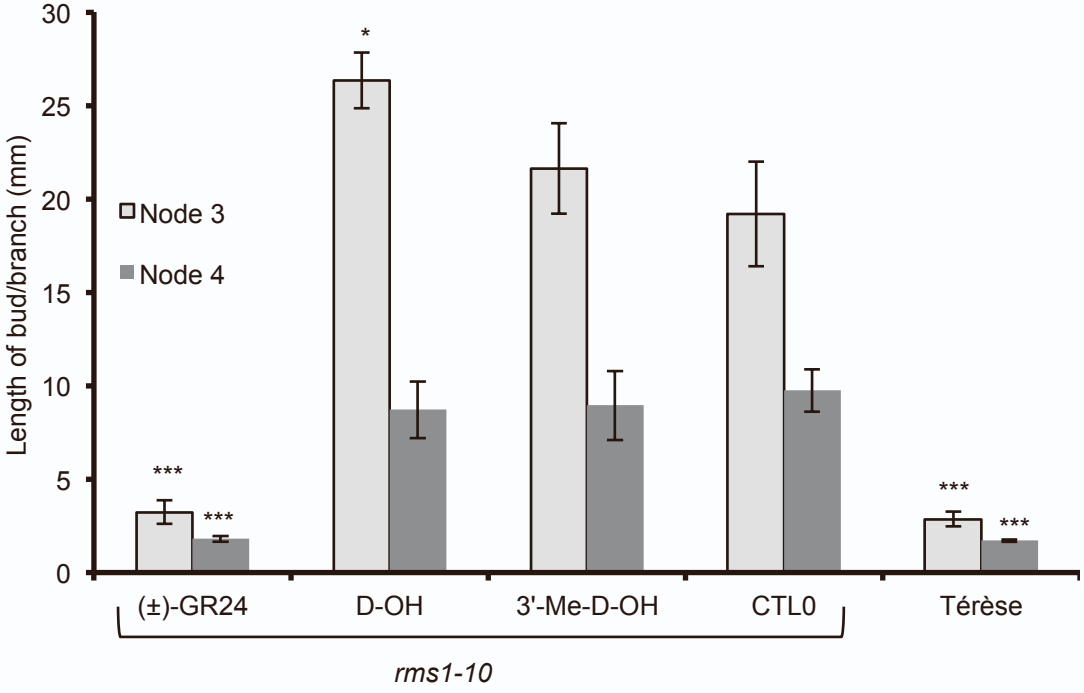

Supplementary Figure 15. Bud outgrowth inhibition activity assay for D derivatives after direct stem infusion. Data are means ± SE (*n* = 12), 8 days after treatment of the pea plants *rms1-10* and Térèse as control. **P* < 0.5, ****P* < 0.001, Kruskal-Wallis rank sum test, compared to control values (CTL0).

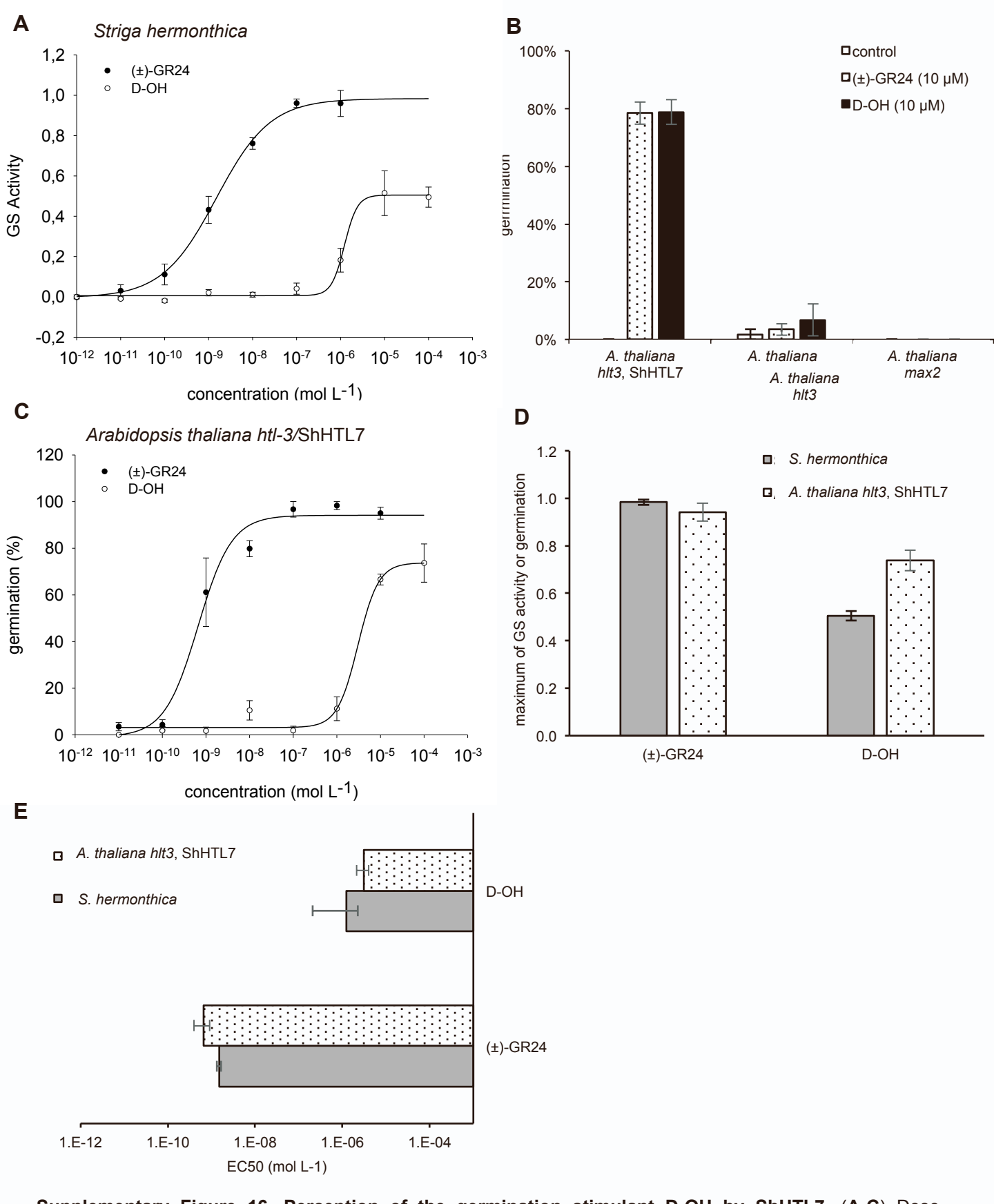

Supplementary Figure 16. Perception of the germination stimulant D-OH by ShHTL7. (**A-C**) Dose response germination stimulation activities and modeled curves of (±)-GR24 and D-OH on seeds of (**A**) *S. hermonthica*, (**C**) *A. thaliana htl-3*, ShHTL7 (34 °C, continuous light for *A. thaliana*). (**B**) Seed germination of *A thaliana htl-3*/ShHTL7, *htl-3* and *max2* with (±)-GR24 and D-OH (10 µM). (**D**) maximum germination stimulation activities and (e) EC_{50} (half maximal effective concentration). Data are indicated ± SE.

Supplementary Table 1. EC_{50} and maximum germination percentage of (+)-GR24, and (−)-GR24 and of (±)-GR24 and D-OH in *Arabidopsis* lines.

species	compound	EC50 (M)	SE	%max	SE
A. thaliana Col-0	(+)-GR24	nd		47%	4%
A. thaliana Col-0	(-)-GR24	1.6E-07	6.4E-08	80%	3%
A. thaliana htl-3	(+)-GR24	nd		9%	1%
A. thaliana htl-3	(-)-GR24	nd		10%	3%
A. thaliana htl-3/p35S::GFP-PrKAI2d3	(+)-GR24	5.9E-12	2.0E-11	75%	1%
A. thaliana htl-3/p35S::GFP-PrKAI2d3	(-)-GR24	4.9E-09	4.2E-09	76%	1%
Striga hermonthica	(±)-GR24	1.5E-09	1.6E-10	98%	1%
Striga hermonthica	D-OH	1.2E-06	1.0E-06	51%	2%
A. thaliana Col-0	(±)-GR24	1.5E-06	4.6E-07	85%	3%
*A. thaliana htl-3/*ShHTL7	(±)-GR24	6.6E-10	2.6E-10	94%	4%
*A. thaliana htl-3/*ShHTL7	D-OH	3.1E-06	9.4E-07	74%	4%

Supplementary Table 2. EC_{50} and maximum of germination stimulant activity of compounds for *P. ramosa*.

compound	EC50 (M)	SE	%max	SE
(+)-GR24	6.5E-12	3.0E-12	100%	5%
(−)-GR24	4.8E-09	2.3E-09	100%	9%
(+)-2'-*epi*-GR24	8.4E-10	2.8E-10	100%	6%
(−)-2'-*epi*-GR24	5.3E-12	2.6E-12	100%	5%
(±)-GR24	4.7E-12	2.6E-12	100%	5%
(±)-Desmethyl-GR24	4.5E-10	2.0E-10	92%	6%
(±)-4'-Desmethyl-2'-*epi*-GR24	9.2E-10	1.8E-10	98%	3%
(±)-3'-Me-GR24	2.6E-09	1.4E-09	95%	9%
(±)-GR24	7.3E-12	3.6E-12	100%	5%
(±)-GC240	4.6E-08	2.9E-08	85%	15%
(±)-GC242	4.7E-09	2.2E-09	94%	8%
(+)-GC242	7.0E-09	2.9E-09	91%	8%
(−)-GC242	6.6E-08	4.7E-08	79%	16%
(±)-GC486	5.7E-08	4.4E-08	97%	22%
DiFMU	nd	nd	3%	2%
YLG	7.7E-09	2.3E-09	91%	6%
(±)-GR24	5.3E-12	3.4E-12	100%	5%
2-PEITC	3.2E-08	2.0E-08	102%	15%
BITC	7.1E-08	2.7E-08	94%	11%
(±)-GR24	5.0E-12	3.1E-12	100%	5%
D-OH	8.3E-09	2.6E-09	86%	5%
D-OEt	nd		27%	14%
D-OMe	nd		39%	21%
D-OsecBu	nd		1%	1%
D-OAll	nd		49%	20%
3'-Me-D-OH	nd		0%	1%
4'-Desmethyl-D-OH	5.0E-08	2.1E-08	101%	8%
Dihydro-D-OEt	nd		32%	18%

Supplementary Table 3. IC_{50} and maximum of inhibition of putative inhibitors of PrKAI2d3 for *P. ramosa*.

	(±)-GR24 (10 nM)				2-PEITC (100 nM)			
compound	IC50(M)	SE	max. inh.	SE	IC50(M)	SE	max. inh.	SE
Soporidine	1.0E-04	8.5E-05	58%	1%	nd		40%	5%
TritonX-100	3.5E-05	6.0E-06	77%	13%	1.5E-05	4.1E-06	94%	6%
KK094	1.4E-05	4.5E-06	100%	2%	5.3E-06	1.3E-06	100%	3%
PMSF	nd		34%	2%	1.0E-04	9.0E-05	57%	20%
TA	nd		31%	9%	1.8E-05	9.5E-06	98%	14%
ABA	1.0E-07	9.4E-09	100%	1%	3.4E-08	2.1E-08	100%	7%

Supplementary Table 4. Oligonucleotides used.

Primer name	purpose	Sequence (5′—3′)	note
Cloning for protein expression			
PrKAI2d3_attb1_HRV3C	PrKAI2d3 coding sequence	ggggacaagtttgtacaaaaaagcaggct*ccctggaagtgctgttttcagggcccg*ATGAACATTAACAGAGACAT	Gene specifics sequences are capitalized Start and Stop codons are highlighted in bold Gateway recombination sites are underlined protease sites are in italic
PrKAI2d3_attb2	PrKAI2d3 coding sequence	ggggaccactttgtacaagaaagctgggtctcaTCAATTAGCATCTGC	
Cloning for complementation assay			
PrKAI2d3_attb2-F		ggggacagctttcttgtacaaagtggcaATGAACATTAACAGAGACATCGG	
PrKAI2d3_attb3-R		ggggacaactttgtataataaagttggATTAGCATCTGCAATATCATG	
PCR-Based mutagenesis			
PrKAI2d3_S98A-F		ctacgtcggccacgctctgtccgccat	
PrKAI2d3_S98A-R		atggcggacagagcgtggccgacgtag	
Q-PCR primer			
PrKAI2c_Fwd1		TGCCACATAATCCAGAGCATGAAG	
PrKAI2c_Rev1		CTAAGAAGCACAGGGACCACAAC	
PrKAI2d1_Fwd2		TGCGACCATTTCTCAAGGACG	
PrKAI2d1_Rev2		GAGATACCGCGACACTTTCACC	
PrKAI2d2_Fwd4		TGACGAATACGGAGGGATACGAAG	
PrKAI2d2_Rev4		TGCGAATCCCAACTGAAAGGAC	
PrKAI2d3_Fwd4		ACTGATCACGATCTCCACTTCCC	
PrKAI2d3_Rev4		CCATCCCCAACACCAATGACTC	
PrKAI2d4_Fwd2		TACGACCCGACATAGCCCTTAG	
PrKAI2d4_Rev2		TACGCCGATTTCGATGCCAC	
PrEF1a_Fwd		TTGCCGTGAAGGATCTGAAAC	

Supplementary Methods

Enzymatic degradation of GR24 isomers by purified proteins. The ligand (10 µM) was incubated without and with purified AtD14/AtKAI2/PrKAI2d3/PrKAI2d3^{S98A} (5 µM) for 150 min at 25ºC in 0.1 mL phosphate buffered saline (PBS; 100 mM Phosphate, pH 6.8, 150 mM NaCl) in the presence of (±)-1-indanol (100 M) as internal standard. The solutions were acidified to pH = 1 by addition of 2 µL trifluoroacetic acid (TFA) to quench the reaction and centrifugated (12 min, 12,000 tr/min). Thereafter, the samples were subjected to reverse-phase-ultra-performance liquid chromatography (RP-UPLC)-MS analyses by means of UPLC system equipped with a Photo Diode Array (PDA) and a Triple Quadrupole Detector (TQD) mass spectrometer (Acquity UPLC-TQD, Waters). RP-UPLC (HSS C_{18} column, 1.8 µm, 2.1 mm × 50 mm) with 0.1% (v/v) formic acid in CH_3CN and 0.1% (v/v) formic acid in water (aq. FA, 0.1%, v/v, pH 2.8) as eluents [10% CH_3CN, followed by linear gradient from 10% to 100% of CH_3CN (4 min)] at a flow rate of 0.6 mL min^{-1}. The detection was done by PDA and with the TQD mass spectrometer operated in Electrospray ionization-positive mode at 3.2 kV capillary voltage. To maximize the signal, the cone voltage and collision energy were optimized to 20 V and 12 eV, respectively. The collision gas was argon at a pressure maintained near 4.5 10^{-3} mBar.

Direct electrospray ionization (ESI)-MS under denaturing conditions. Mass spectrometry measurements were carried out with an electrospray quadrupole-time of flight (Q-TOF) mass spectrometer (Waters) equipped with the Nanomate device (Advion). The HD_A_384 chip (5 µm i.d. nozzle chip, flow rate range 100−500 nL/min) was calibrated before use. For the ESI−MS measurements, the Q-TOF instrument was operated in radio frequency quadrupole mode with the TOF data collected between *m/z* 400−2990. The collision energy was set to 10 eV and argon was used as collision gas. Mass spectra were acquired after denaturation of PrKAI2d3/PrKAI2d3^{S98A} [(50 µM in ammonium acetate buffer (50 mM, pH 6.8)] ± ligand in 50% (v/v) acetonitrile and 1% (v/v) formic acid. The Mass Lynx 4.1 (Waters) and Peakview 2.2 (AB Sciex) softwares were used for data acquisition and processing, respectively. Multiply-charged ions were deconvoluted by the MaxEnt algorithm (AB Sciex). The protein average masses were annotated in the spectra and the estimated mass accuracy was ± 2 Da. For the external calibration, NaI clusters (2 µg/µL, isopropanol/H_2O 50/50, Waters) were used in the acquisition *m/z* mass range.

Localization of the fixation site of ligands on PrKAI2d3. PrKAI2d3-ligand mixtures were incubated for 10 min prior overnight Glu-C proteolysis. Glu-C--generated peptide mixtures were analyzed by nanoLC-MS/MS with the Triple-TOF 4600 mass spectrometer (AB Sciex) coupled to the nanoRSLC UPLC system (Thermo Fisher Scientific) equipped with a trap column (Acclaim PepMap 100 C_{18}, 75 µm i.d. × 2 cm, 3 µm) and an analytical column (Acclaim PepMap RSLC C_{18}, 75 µm i.d. × 25 cm, 2 µm, 100 Å). Peptides were loaded at 5 µL/min with 0.05% (v/v) TFA in 5% (v/v) acetonitrile and separated at a flow rate of 300 nL/min with a 5% to 35% solvent B [0.1% (v/v) formic acid in 100% acetonitrile] gradient in 40 min with solvent A [0.1% (v/v) formic acid in water]. NanoLC-MS/MS experiments were conducted in a Data-Dependent acquisition method by selecting the 20 most intense precursors for collision-induced dissociation fragmentation with the Q1 quadrupole set at a low resolution for better sensitivity. Raw data were processed with the MS Data Converter tool (AB Sciex) for generation of .mgf data files and proteins were identified with the MASCOT search engine (Matrix Science) against the PrKAI2 sequence with oxidation of methionines and ligand-histidine adduct as variable modifications. Peptide and

fragment tolerance were set at 20 ppm and 0.05 Da, respectively. Only peptides were considered with a MASCOT ion score above the identity threshold (25) calculated at 1% false discovery rate.

Protein melting temperatures. For the Differential Scanning Fluorimetry (DSF) experiments a CFX96 Touch^{TM} Real-Time PCR Detection System (Bio-Rad) was used with excitation and emission wavelengths of 490 and 575 nm, respectively and Sypro Orange ($\lambda_{ex}/\lambda_{em}$: 470/570 nm; Life Technologies) as the reporter dye. Samples were heat-denatured with a linear 25 °C to 95 °C gradient at a rate of 1.3 °C per min after incubation at 25 °C for 30 min in the dark. The denaturation curve was obtained by means of the CFX manager™ software. Final reaction mixtures were prepared in triplicate in 96-well white microplates. Each reaction was carried out in 20-µL sample in PBS (100 mM phosphate, pH 6.8, 150 mM NaCl) containing 6 µg of protein (so that the final reactions contained 10 µM protein), 0 to X ligand concentrations in µM, 4% (v/v) DMSO, and 0.008 µL Sypro Orange. Plates were incubated in the dark for 30 min before analysis. In the control reaction, DMSO was added instead of the chemical solution. The experiments were repeated three times.

Plant material and growth conditions. Pea (*Pisum sativum*) branching mutant plants were derived from various cultivars after ethyl methanesulfonate (EMS) mutagenesis and had been described previously (Rameau et al., 1997). The *rms1-10* (M3T-884) mutant was obtained from the dwarf cv Térèse. Plants were grown in a greenhouse under long-day as described (Braun et al., 2012).
All *Arabidopsis thaliana* (L.) Heynh. mutant plants (Columbia-0 [Col-0] accession background) have been described previously: *htl-3* (ref. (Toh et al., 2014a; Toh et al., 2014b)), *Atd14-1/htl-3* (ref. (Toh et al., 2014a; Toh et al., 2014b)), and *htl-3* ShHTL7 (kind gift of P. McCourt). For overexpression of the green fluorescent protein (GFP) fusions of PrKAI2d3 and PrKAI2d3^{S98A}, transgenic *Arabidopsis* seeds were generated by the *Agrobacterium* floral dip method (Clough and Bent, 1998) with the *htl-3* mutant as the background accession. Transgenic seeds were selected based on the antibiotic resistance and GFP fluorescence.

Pea shoot-branching assay. The compounds to be tested were applied by vascular supply. The control was the treatment with 0.1% dimethylsulfoxide (DMSO) only. Twelve plants were sown per treatment in trays and generally 10 days after sowing the axillary bud at node 3 was treated. Compounds in DMSO solution were diluted in water to the indicated concentrations for a treatment with 0.1% (v/v) DMSO. The branches at nodes 1 and 2 were removed to encourage the outgrowth of axillary buds at the nodes above. Nodes were numbered acropetally from the first scale leaf as node 1 and cotyledonary node as node 0. Bud growth at nodes 3 and 4 was measured with digital callipers 8 to 10 days after treatment. Plants with damaged main shoot apex or with a dead white treated-bud were discarded from the analysis. The SL-deficient *rms1-10* pea mutant was used for all experiments.

General experimental procedures for synthetic chemistry

All non-aqueous reactions were run under an inert atmosphere (argon), by using standard techniques for manipulating air-sensitive compounds. All glassware was stored in the oven and/or was flame-dried prior to use. Anhydrous solvents were obtained by filtration through drying columns. Analytical thin-layer chromatographies (TLC) were performed on plates precoated with silica gel layers. Compounds were visualized by one or more of the following methods: (1) illumination with a short wavelength UV lamp (i.e., λ = 254 nm), (2) spray with

a $KMnO_4$ solution in H_2O. Flash column chromatography was performed using 40-63 mesh silica. Nuclear magnetic resonance spectra (^1H; ^{13}C NMR) were recorded respectively at [500; 125] MHz on a Bruker DPX 500 spectrometer. For the ^1H spectra, data are reported as follows: chemical shift, multiplicity (s = singlet, d = doublet, t = triplet, q = quartet, m = multiplet, bs = broad singulet, coupling constant in Hz and integration. IR spectra are reported in reciprocal centimeters (cm^{-1}). Mass spectra (MS) and high-resolution mass spectra (HRMS) were determined by electrospray ionization (ESI) coupled to a time-of-flight analyser (Waters LCT Premier XE).

Preparation of GR24 isomers, probes, and other ligands. For general experimental procedures, see the Supplementary Methods. (±)-2'-*epi*-GR24 and (±)-GR24 were prepared as described (Mangnus et al., 1992) and (±)-4'-desmethyl-GR24, (±)-2'-*epi*-4'-desmethyl-GR24, and (±)-3'-Me-GR24 as described (Boyer et al., 2012). (+)-GR24, (−)-GR24, (+)-2'-*epi*-GR24, and (−)-2'-*epi*-GR24 were separated from (±)-2'-*epi*-GR24 and (±)-GR24 by chiral supercritical fluid chromatography as described (de Saint Germain et al., 2016; de Saint Germain et al., 2019). (±)-GR24 was purified by semi-preparative HPLC by means of a Interchim puriFlash® 4250 instrument, combined with a fraction collector with integrated ELSD, a PDA and a Phenomenex Luna C18, 250 × 21.2 mm, 5-µm column (H_2O/CH_3CN: 6/4) or Interchim Uptisphere Strategy SI, 250 × 21.2 mm, 5-µm column (Heptane/EtOAc: 1/1). 2-Phenethyl isothiocyanate (2-PEITC), benzylisothiocyanate (BEITC), DiFMU, *para*-nitrophenyl acetate (*p*-NPA), Yoshimulactone Green (YLG), abscisic acid (ABA), tolfenamic acid (Hamiaux et al., 2018) (TA), TritonX-100 (Shahul Hameed et al., 2018) and phenylmethylsulfonyl fluoride (PMSF) are commercially available. KK094 (Nakamura et al., 2019) and soporidine (Holbrook-Smith et al., 2016) were kindly provided by T. Asami and P. McCourt (University of Toronto), respectively. Probes (GC486, GC240, and GC242) were prepared as described (de Saint Germain et al., 2016).

Preparation of GR24 isomers

(±)-2'-*epi*-GR24 and (±)-GR24 were prepared according to described procedures (Mangnus et al., 1992). ((+)-GR24, (−)-GR24, (+)-2'-*epi*-GR24, (−)-2'-*epi*-GR24 were separated from (±)-2'-*epi*-GR24 and (±)-GR24 by chiral supercritical fluid chromatography as described in (de Saint Germain et al., 2016). (±)-GR24 can be purified by semi-preparative HPLC. Semi-preparative HPLC was performed using a Interchim puriFlash® 4250 instrument, combined with a fraction collector with integrated ELSD, a PDA and a Phenomenex Luna C18, 250 × 21.2 mm, 5 µm column (H_2O/CH_3CN : 6 /4) or Interchim Uptisphere Strategy SI, 250 × 21.2 mm, 5 µm column (Heptane/EtOAc : 1 /1).

Preparations of D-OH and analogs

(±)-D-OH was prepared according to Fell & Harbridge (Fell and Harbridge, 1990). (±)-3'-Methyl-D-OH was prepared according to Canévet & Graff (Canévet and Graff, 1978).

Preparation of (±)-D-OEt (Bayer et al., 2016; Wigchert and Zwanenburg, 1999) **by a modification of the Bayer et al. procedure** (Bayer et al., 2016)

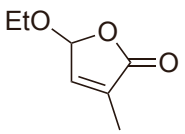

To a 0 °C solution of $TiCl_4$ (16.5 mL, 150 mmol) in anhydrous CH_2Cl_2 (212 mL) was added dropwise under argon a mixture of ethyl pyruvate (16.5 mL, 150 mmol) and vinyl acetate (16.5 mL, 150 mmol) in anhydrous CH_2Cl_2 (106 mL). When addition is complete, the suspension was further stirred for 2 hours at 0 °C. The reaction mixture was quenched with H_2O (140 mL). The aqueous solution was extracted with CH_2Cl_2 (2 × 100 mL). The combined organic layers were washed with H_2O (100 mL), brine (100 mL), dried (Na_2SO_4), filtered and evaporated under

reduced pressure. The residue (30 g) was diluted in EtOH (345 mL), AcOH (17 mL), conc. HCl (17 mL) and stirred under reflux for 4 hours. EtOH was removed by distillation and the cooled residue was extracted with EtOAc (3 × 150 mL). The combined organic layers were washed with brine, dried (Na_2SO_4), filtered and evaporated under reduced pressure. The residue was distilled (120-130 °C) with Kugelrohr to give (±)-D-OEt (Wigchert and Zwanenburg, 1999) as a pale yellow liquid (9.3 g, 65.5 mmol, 44%).

Preparation of (±)-D-OMe (Chapleo et al., 1976)

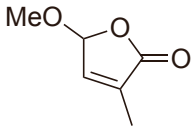

A mixture of (±)-D-O-Et (1.00 g, 7.04 mmol) and *para*-toluene sulfonic acid (250 mg, 1.31 mmol) in MeOH (44 mL) was stirred for 48 h at room temperature. MeOH was removed under reduced pressure and the residue was diluted with EtOAc (50 mL). The organic solution was washed with a $NaHCO_3$ saturated aqueous solution, brine, dried ($MgSO_4$), filtered and evaporated under reduced pressure. The residue was distilled (1 mm Hg, 70-110 °C) with Kugelrohr to give (±)-D-OMe (Chapleo et al., 1976) as a colourless liquid (0.81 g, 6.33 mmol, 90%).

Preparation of (±)-Dihydro-D-OEt

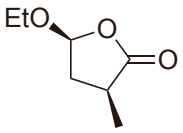

A solution of (±)-D-OEt (Wigchert and Zwanenburg, 1999) (429 mg, 3.02 mmol) and 10% Pd/C (170 mg) in EtOAc (45 mL) was stirred under H_2 atmosphere for 75 min at room temperature, flushed with argon and filtered on Celite. The resultant solution was evaporated under reduced pressure and distilled (1 mm Hg, 80-90 °C) with Kugelrohr to give (±)-Dihydro-D-OEt (Redon et al., 2008) as a colourless liquid (266 mg, 1.84 mmol, 61%).

Preparation of (±)-Dihydro-D-O*sec*-Bu

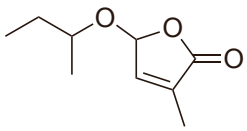

A mixture of (±)-D-O-Et (2.02 g, 14.02 mmol) and *para*-toluene sulfonic acid (503 mg) in *sec*-BuOH (40 mL) was stirred for 3 h at reflux. *sec*-BuOH was removed under reduced pressure and the residue was diluted with EtOAc (200 mL). The organic solution was washed with a 5% $NaHCO_3$ aqueous solution (2 × 50 mL), dried ($MgSO_4$), filtered and evaporated under reduced pressure. The residue was distilled (1 mm Hg, 70-110 °C) with Kugelrohr to give (±)-D-O*sec*-Bu as a colourless liquid (1.11 g, 6.52 mmol, 46%). Mixture of 2 diastereomers (1:1). ^{1}H NMR ($CDCl_3$, 300 MHz): δ (ppm) 0.87 (t, J = 7.5 Hz, 3H), 0.90 (t, J = 7.5 Hz, 3H), 1.19 (d, J = 6.0 Hz, 3H), 1.23 (d, J = 6.0 Hz, 3H), 1.44-1.64 (m, 4H), 1.89-1.91 (m, 6H), 3.75-3.85 (m, 2H), 5.81-5.83 (m, 1H), 5.83-5.86 (m, 1H), 6.73-6.76 (m, 2H). ^{13}C NMR ($CDCl_3$, 75 MHz): δ (ppm) 9.7 (CH_3), 9.8 (CH_3), 10.72 (CH_3), 10.76 (CH_3), 19.4 (CH_3), 20.9 (CH_3), 29.5 (CH_2), 29.9 (CH_2), 77.5 (CH), 77.9 (CH), 100.2 (CH), 101.7 (CH), 133.9 (2C), 143.3 (CH), 143.5 (CH), 172.28 (C), 172.30 (C). HRMS (ESI): Calculated for $C_9H_{15}O_3$ $[M + H]^+$: 171.1021. Found: 171.1019.

Preparation of (±)-Dihydro-D-OAll

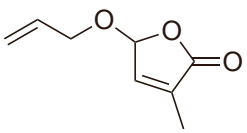

A mixture of (±)-D-O-Et (1.01 g, 7.13 mmol) and *para*-toluene sulfonic acid (250 mg, 1.31 mmol) in allylic alcohol (40 mL) was stirred for 24 h at room temperature. Allylic alcohol was removed under reduced pressure and the residue was diluted with EtOAc (100 mL). The organic solution was washed with a 5% $NaHCO_3$ aqueous solution (2 × 50 mL), dried ($MgSO_4$), filtered and evaporated under reduced pressure. The residue was distilled (20 mm Hg, 90 °C) with Kugelrohr to give (±)-D-OAll as a colourless liquid (719 mg, 4.66 mmol, 65%). ^{1}H NMR ($CDCl_3$, 300 MHz): δ (ppm) 1.90 (s, 3H), 4.16 (dd, J = 12.5, 6.5 Hz, 1H), 4.32 (dd, J = 12.5, 5.5 Hz, 1H), 5.22 (d, J = 10.5 Hz, 1H), 5.30 (dd, J = 17.0, 3.0 Hz,

1H), 5.79-5.81 (bs, 1H), 5.82-5.95 (m, 1H), 6.78-6.79 (bs, 1H). ^{13}C NMR ($CDCl_3$, 75 MHz): δ (ppm) 10.7 (CH_3), 70.8 (CH_2), 100.7 (CH), 119.0 (CH_2), 133.0 (CH), 134.3 (C), 143.0 (CH), 172.0 (C). IR (film): ν (cm^{-1}) 3085, 2983, 2928, 1764, 1668, 1649. HRMS (ESI): Calculated for $C_8H_{11}O_3$ $[M + H]^+$: 155.0708. Found: 155.0703.

Preparation of (±)-4'-desmethyl-D-OH

To a solution of (±)-4'-desmethyl-D-Br (Wolff and Hoffmann, 1988) (200 mg, 1.23 mmol) was added an aqueous solution of KOH (2 mL, 2 M). The resultant mixture was stirred at room temperature for 2 h, neutralized with an aqueous solution of HCl (1 M) and extracted with EtOAc (3 × 15 mL). The combined organic layers were dried (Na_2SO_4), filtered and evaporated under reduced pressure. The residue was chromatographied on silica gel (Heptane/ EtOAc 100:0 to 1:1) to give (±)-4'-desmethyl-D-OH (Byun et al., 2018) as a white solid (45 mg, 37%).

References

Bayer, T.S., Davidson, E.A., and Hleba, Y. (2016). Methods for hydraulic enhancement of crops. PCT/US2016/029080.

Boyer, F.-D., de Saint Germain, A., Pillot, J.-P., Pouvreau, J.-B., Chen, V.X., Ramos, S., Stévenin, A., Simier, P., Delavault, P., Beau, J.-M., et al. (2012). Structure-Activity Relationship Studies of Strigolactone-Related Molecules for Branching Inhibition in Garden Pea: Molecule Design for Shoot Branching. Plant Physiol. 159:1524-1544.

Braun, N., de Saint Germain, A., Pillot, J.P., Boutet-Mercey, S., Dalmais, M., Antoniadi, I., Li, X., Maia-Grondard, A., Le Signor, C., Bouteiller, N., et al. (2012). The pea TCP transcription factor PsBRC1 acts downstream of Strigolactones to control shoot branching. Plant Physiol. 158:225-238.

Byun, J., Huang, W., Wang, D., Li, R., and Zhang, K.A.I. (2018). CO2 -Triggered Switchable Hydrophilicity of a Heterogeneous Conjugated Polymer Photocatalyst for Enhanced Catalytic Activity in Water. Angew. Chem. Int. Ed. 57:2967-2971.

Canévet, J.C., and Graff, Y. (1978). Réactions de Friedel-Crafts de dérivés aromatiques sur des composés dicarbonylés-1,4éthyléniques-2,3.II Alkylations par quelques hydroxy-5 ou chloro-5 dihydro-2,5 furannones-2. Nouvelle méthode de synthèse des acides 1H-indènecarboxyliques-1. Tetrahedron 34:1935-1942.

Chapleo, C.B., Svanholt, K.L., Martin, R., and Dreiding, A.S. (1976). Synthesis of Bromo-substituted 2-Buten- and 2-Penten-4-olides. Helv. Chim. Acta 59:100-107.

Clough, S.J., and Bent, A.F. (1998). Floral dip: a simplified method for Agrobacterium-mediated transformation of *Arabidopsis thaliana*. Plant J. 16:735-743.

de Saint Germain, A., Clavé, G., Badet-Denisot, M.-A., Pillot, J.-P., Cornu, D., Le Caer, J.-P., Burger, M., Pelissier, F., Retailleau, P., Turnbull, C., et al. (2016). An histidine covalent receptor and butenolide complex mediates strigolactone perception. Nat. Chem. Biol. 12:787-794.

de Saint Germain, A., Retailleau, P., Norsikian, S., Servajean, V., Pelissier, F., Steinmetz, V., Pillot, J.-P., Rochange, S., Pouvreau, J.-B., and Boyer, F.-D. (2019). Contalactone, a contaminant formed during chemical synthesis of the strigolactone reference GR24 is also a strigolactone mimic. Phytochemistry 168:112112.

Fell, S.C.M., and Harbridge, J.B. (1990). 2,5-dimethoxy-2,5-dihydrofuran: A convenient synthon for a novel mono-protected glyoxal; synthesis of 4-hydroxybutenolides. Tetrahedron Lett. 31:4227-4228.

Hamiaux, C., Drummond, R.S.M., Luo, Z.W., Lee, H.W., Sharma, P., Janssen, B.J., Perry, N.B., Denny, W.A., and Snowden, K.C. (2018). Inhibition of strigolactone receptors

by N-phenylanthranilic acid derivatives: Structural and functional insights. J. Biol. Chem. 293:6530-6543.
Holbrook-Smith, D., Toh, S., Tsuchiya, Y., and McCourt, P. (2016). Small-molecule antagonists of germination of the parasitic plant *Striga hermonthica*. Nat. Chem. Biol. 12:724-729.
Mangnus, E.M., Dommerholt, F.J., Dejong, R.L.P., and Zwanenburg, B. (1992). Improved Synthesis of Strigol Analog GR24 and Evaluation of the Biological-Activity of Its Diastereomers. J. Agric. Food. Chem. 40:1230-1235.
Nakamura, H., Hirabayashi, K., Miyakawa, T., Kikuzato, K., Hu, W., Xu, Y., Jiang, K., Takahashi, I., Niiyama, R., Dohmae, N., et al. (2019). Triazole Ureas Covalently Bind to Strigolactone Receptor and Antagonize Strigolactone Responses. Mol. Plant 12:44-58.
Rameau, C., Bodelin C, Cadier D, Grandjean O, Miard F, and Murfet IC. (1997). New *ramosus* mutants at loci *Rms1*, *Rms3* and *Rms4* resulting from the mutation breeding program at Versailles. Pisum Genetics 29:7-12.
Redon, S., Pannecoucke, X., Franck, X., and Outurquin, F. (2008). Synthesis and oxidative rearrangement of selenenylated dihydropyrans. Org. Biomol. Chem. 6:1260-1267.
Shahul Hameed, U., Haider, I., Jamil, M., Kountche, B.A., Guo, X., Zarban, R.A., Kim, D., Al-Babili, S., and Arold, S.T. (2018). Structural basis for specific inhibition of the highly sensitive ShHTL7 receptor. EMBO Rep. 19:e45619.
Toh, S., Holbrook-Smith, D., Stokes, M.E., Tsuchiya, Y., and McCourt, P. (2014a). Detection of Parasitic Plant Suicide Germination Compounds Using a High-Throughput Arabidopsis HTL/KAI2 Strigolactone Perception System. Chem. Biol. 21:988-998.
Toh, S., Holbrook-Smith, D., Stokes, Michael E., Tsuchiya, Y., and McCourt, P. (2014b). Erratum. Chem. Biol. 21:1253.
Wigchert, S.C.M., and Zwanenburg, B. (1999). A critical account on the reception of Striga seed germination. J. Agric. Food. Chem. 47:1320-1325.
Wolff, S., and Hoffmann, H.M.R. (1988). Aflatoxins revisited - convergent synthesis of the ABC-moiety. Synthesis:760-763.